

CHAPTER 1

INTRODUCTION

From time immemorial, wind has been harnessed to move ships and large boats, till the introduction of steam engines. Initially, wind was used to drive sails so that the vehicles move forward. In several countries of the world, using sails and capturing wind energy for moving over water still persists, but is mostly used for leisurely activities such as windsurfing, yachting, sailing ships and boats. However, today with so much pollution and the problem of global warming facing us, scientists have thought of and devised ways of developing a wind car. It hasn't grown to that big an industry like thermal or hydroelectricity generation, but has still been able to create a niche for itself.

The wind car is the kind of car powered by natural wind energy. The main objective is to convert the wind energy to mechanical energy to rotate the main shaft. The basic task is conversion and storage of wind energy. There are many way to convert and store wind energy to mechanical energy. This involves:

- Use generator: the turbine will rotate the rotor connected to the windings of the generator, thereby creating a magnetic flux which in turn produces an induced current that help charges the battery that supplies the main power to be used.
- Use hydraulic compressors: here, the turbine will rotate and hydraulically compress a working fluid (generally gas) which helps store the energy and later expands to rotate the turbine when needed.
- Direct use of fly wheel: a fly wheel is a disk of mass that helps store the energy from a rotating torque at constant rate.
- Direct connection to the wheel: in this complex method the turbine is directly connected to the wheels by the use of various kinds of links and gear.

Calculations are very important and sensitive to this project referred to chapter 2. The purpose of this project is to calculate and analyze pressure and velocity distribution around an airfoil, to

calculate lift and drag. For this reason computer programming (matlab) has been written and used for most of the calculation.

The remaining chapters of this thesis are organized, as follows; Chapter two reviews the complete mathematical modeling to calculate the design parameters of airfoil is presented. The model is based on the aerofoil theory. The third chapter reviews and describes the methodology of some numerical solutions examined and applied to calculate the parameter of the airfoils.

The forth chapter presents the results of the thesis. And the fifth chapter concludes the thesis and presents the probable future development of this work.

CHAPTER 2

AIRFOIL THEORY

The airfoil shape is expressed analytically as a function of some design parameters. The NACA four and five digits is used with design parameters that control the camber and the thickness of the airfoil. The inviscid flow is computed with a linear vortex panel method, which provides the lift and moment coefficients. The boundary layer is computed using an integral formulation. In this chapter, a complete mathematical modeling to calculate the design parameters of the airfoil is presented.

2.1 Airfoil Geometry Parameters

If a horizontal wing is cut by a vertical plane parallel to the centerline of the vehicle, the resultant section is called the airfoil section. The generated lift and the stall characteristics of the wing depend strongly on the geometry of airfoil section that make up the wing. Geometric parameters that have an important effect on the aerodynamic characteristic of an airfoil section include

- 1) The leading-edge radius.
- 2) The mean camber line.
- 3) The maximum thickness and the thickness distribution of the profile.
- 4) The trailing-edge angle.

The effect of these parameters, which are illustrated in figure 2.1 will be discussed after a brief introduction to airfoil-section nomenclature. [1]

2.1.1 Airfoil-Section Nomenclature

The geometry of many airfoil sections is uniquely defined by the NACA designation for the airfoil. There are a variety of classifications, including NACA four digit wing sections, NACA five digit wing sections, and NACA six digit wing sections.

As an example, consider the four- digit wing section. The first integer indicates the maximum value of the mean camber-line ordinate (see figure 2.1) in percent of the chord. The second integer indicates the distance from the leading edge to the maximum camber in tenth of the chord. The last two integers indicate the maximum section thickness in percent of the chord.

Thus the NACA 0012 is a symmetric airfoil section whose maximum thickness is 12 percent of the chord. The NACA 4412 airfoil section is a 12 percent thick airfoil which has 4 percent maximum camber located at 40 percent of the chord. [1]

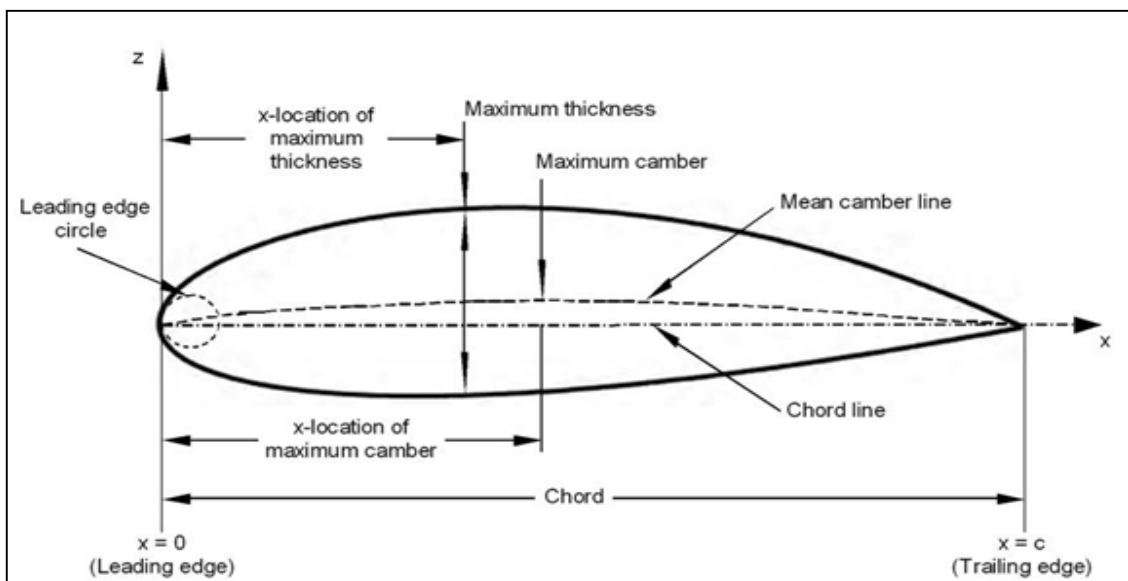


Figure 2.1 Airfoil-section geometry and its nomenclature. [2]

2.1.2 Leading-Edge (LE) and Chord Line

The chord of an airfoil is an imaginary straight line drawn through the airfoil from its leading edge to its trailing edge. We might think of this chord line as the starting point for drawing or designing an airfoil in cross section. It is from this baseline that we determine how much upper or lower camber there is and how wide the wing is at any point along the wingspan. The leading edge of an airfoil is the portion that meets the air first. The shape of the leading edge depends upon the function of the airfoil. If the airfoil is designed to operate at high speed, its leading edge

will be very sharp, as on most current fighter aircraft, if the airfoil is designed to produce a greater amount of lift at a relatively low rate of speed. [3]

2.1.3 Mean Camber Line

The mean camber line of an airfoil is the line from the leading edge to the trailing edge, of which each point lies exactly halfway between the upper and lower surfaces. For an airfoil with zero camber (i.e., the wing is symmetric about the chord line), the mean camber line is straight and corresponds to the chord line. In other cases, the mean camber line is curved. [4]

2.1.4 Maximum Thickness and Thickness Distribution

The maximum thickness and thickness distribution strongly influence the aerodynamic characteristic of the airfoil section as well. The maximum local velocity to which a fluid particle accelerates as it flows around an airfoil section increases as the maximum thickness increases. Thus the minimum pressure value is smallest for the thickest airfoil section. As the result, the adverse pressure gradient associated with the deceleration on the flow from the location of this pressure minimum to the trailing edge is greatest for the thickest airfoil. As the adverse pressure gradient becomes larger, the boundary layer becomes thicker (and is more likely to separate producing relatively large values for the form drag). Thus, the beneficial effects of increasing the maximum thickness are limited.

For a very thin airfoil section (which has relatively small leading edge radius), boundary layer separation occurs early, not far from the leading edge of the upper surface. As result, the maximum section lift coefficient for a very thin airfoil section is relatively small.

The thickness distribution for airfoil affects the pressure distribution and the character of the boundary layer. As the location of the maximum thickness moves aft, the velocity gradient (and hence pressure gradient) in the mid chord region decreases.

The resultant favorable pressure gradient in the mid chord region promotes boundary layer stability and increases the possibility that the boundary layer remains laminar. Laminar boundary layers produce less skin friction drag than turbulent boundary layer but are also more likely to separate under the influence of an adverse pressure gradient.

In addition, the thicker airfoils benefit more from the use of high lift devices but have lower critical Mach number. [3]

2.1.5 Trailing-Edge Angle (TE)

The trailing edge is the back of the airfoil, the portion at which the airflow over the upper surface joins the airflow over the lower surface. The design of this portion of the airfoil is just as important as the design of the leading edge. This is because the air flowing over the upper and lower surfaces of the airfoil must be directed to meet with as little turbulence as possible, regardless of the position of the airfoil in the air. [3]

2.2 NACA Airfoil

The NACA airfoils are airfoil shapes for aircraft wings developed by the National Advisory Committee for Aeronautics (NACA). The shape of the NACA airfoils is described using a series of digits following the word "NACA." The parameters in the numerical code can be entered into equations to precisely generate the cross-section of the airfoil and calculate its properties as shown in figure 2.2.

2.2.1 Four-digit Series

The NACA four-digit wing sections define the profile by:

1. One digit describing maximum camber as percentage of the chord.
2. One digit describing the distance of maximum camber from the airfoil leading edge in tens of percents of the chord.
3. Two digits describing maximum thickness of the airfoil as percent of the chord.

The formula for the shape of a NACA 00XX foil, with "XX" being replaced by the percentage of thickness to chord, is:

$$z = \frac{t/c}{0.2} c \left[a \sqrt{\frac{x}{c}} - b \left(\frac{x}{c}\right) - c \left(\frac{x}{c}\right)^2 + d \left(\frac{x}{c}\right)^3 - e \left(\frac{x}{c}\right)^4 \right] \quad 2.1a$$

where

- $a = 0.2969$
- $b = 0.126$
- $c = 0.3516$
- $d = 0.2843$
- $e = 0.1015$
- z is the half thickness at a given value of x , and
- t/c is relative thickness (thickness ratio)

and also the eq.2.1a can be in dimensionless form

$$z = \frac{t/c}{0.2} c [a\sqrt{X} - b(X) - c(X)^2 + d(X)^3 - b(X)^4] \quad 2.1b$$

Where:

- $X = \frac{x}{c}$
- c is the chord length,
- x is the position along the chord from 0 to c ,

Now the coordinates (x_U, z_U) of the upper airfoil surface, and (x_L, z_L) of the lower airfoil surface are:

$$x_U = x_L = x, \quad z_U = +z, \text{ and } z_L = -z$$

The simplest asymmetric foils are the NACA 4-digit series foils, which use the same formula as that used to generate the 00XX symmetric foils, but with the line of mean camber bent. The formula used to calculate the mean camber line is:

$$z_c = \begin{cases} h \frac{x}{x_h^2} \left(2x_h - \frac{x}{c} \right) & , \text{ from } x = 0 \text{ to } x = x_h c \\ h \frac{c-x}{(1-x_h)^2} \left(1 + \frac{x}{c} - 2x_h \right) & , \text{ from } x = x_h c \text{ to } x = c \end{cases} \quad 2.2$$

Where:

- h is the maximum camber,
- x_h is the location of maximum camber.

2.2.2 Five-digit Series

The NACA five-digit series describes more complex airfoil shapes:

1. The first digit, when multiplied by 0.15, gives the designed coefficient of lift (C_L).
2. Second and third digits, when divided by 2, give p , the distance of maximum camber from the leading edge (as per cent of chord).
3. Fourth and fifth digits give the maximum thickness of the airfoil (as per cent of the chord).

For example, the NACA 12018 airfoil would give an airfoil with maximum thickness of 18% chord, maximum camber located at 10% chord, with a lift coefficient of 0.15

The camber-line is defined in two sections:

$$z_c = \begin{cases} \frac{k_1}{6}(x^3 - 3hx^2 + h^2(3-h)x) & , \quad 0 < x < x_h \\ \frac{k_1 h}{6}(1-x) & , \quad x_h < x < 1 \end{cases} \quad 2.3$$

Where the chord wise location x and the ordinate y have been normalized by the chord. The constant h is chosen so that the maximum camber occurs at $x = x_h$; for example, the NACA 13012 has camber-line 230, $x_h = 0.3 / 2 = 0.15$ and $h = 0.2025$. Finally, constant k_1 is determined to give the desired lift coefficient; for camber-line 230 again, $k_1 = 15.957$ is used. [5]

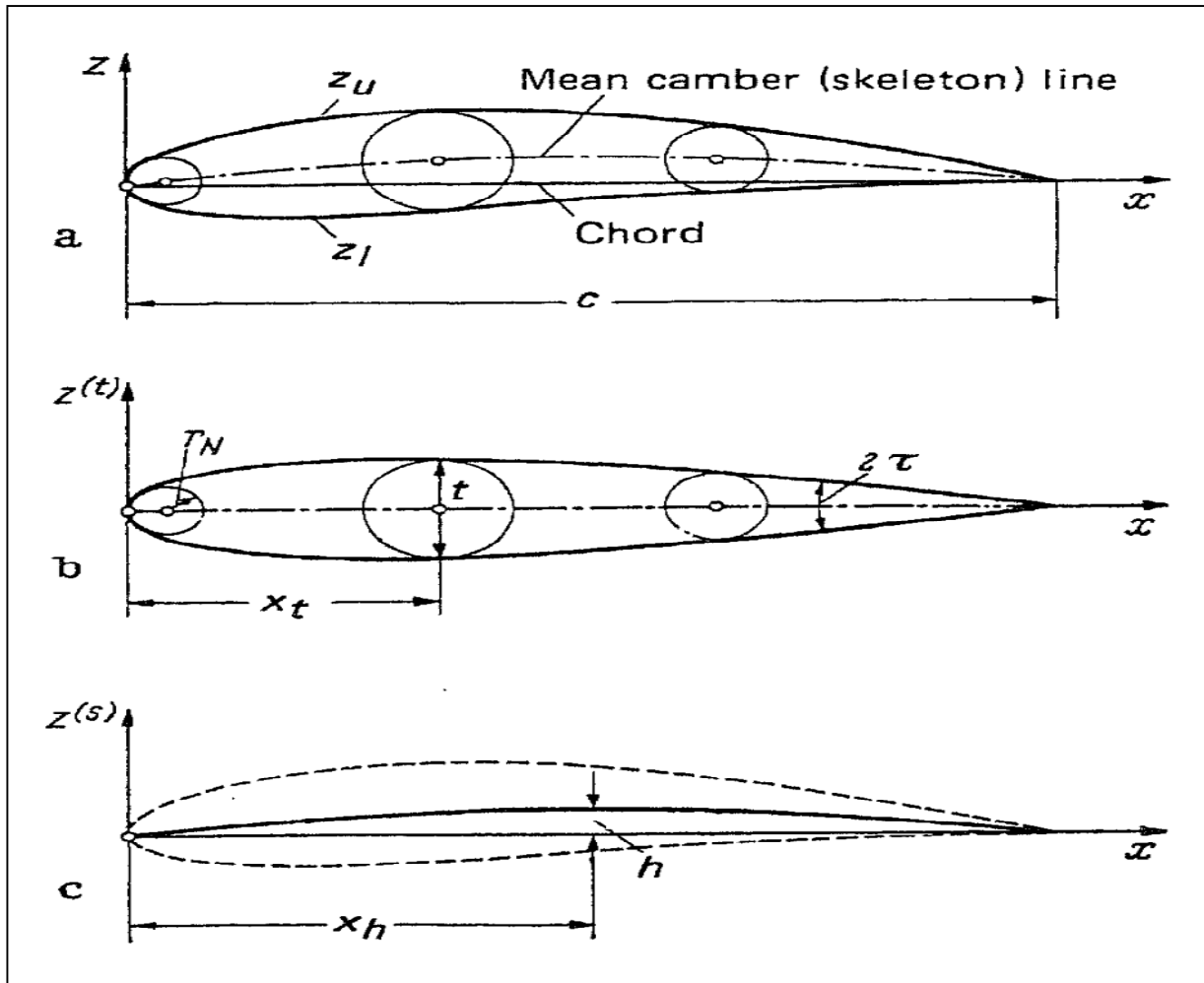


Figure 2.2 Geometric terminology of lifting wing profiles, (a) Total profile, (b) Profile teardrop (thickness distribution). (c) Mean camber (skeleton) line (camber height distribution). [6]

t/c	relative thickness (thickness ratio)
h/c	relative camber (camber ratio)
x_t/c	relative thickness position
x_h/c	relative camber position
r_N/c	relative nose radius
2τ	trailing edge angle

2.3 Vortex Filament

Consider 2-D/point vortices of same strength duplicated in every plane parallel to the z-x plane along the y-axis from $-\infty$ to ∞ . The flow is 2-D and is irrotational everywhere except the y-axis. y-axis is the straight vortex filament and may be defined as a line.

Vortex filament is a straight or curved line in a fluid which coincides with the axis of rotation of successive fluid elements. [7]

2.4 Helmholtz's Vortex Theorems

The strength of a vortex filament is constant along its length. A vortex filament induces a velocity field that is irrotational at every point excluding the filament. If we enclose a vortex filament with a sheath from which a slit has been removed, the vorticity at every point on the surface until be zero. If we evaluate the circulation for the sheath. as

$$\Gamma = -\oint_C \vec{V} \cdot d\vec{s} = -\iint_A (\nabla \times \vec{V}) \cdot d\vec{A} \quad 2.4$$

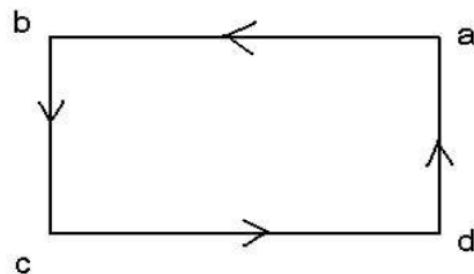
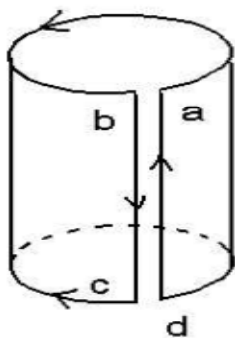
where

$$\nabla \times \vec{V} = 0, \quad -\oint_C \vec{V} \cdot d\vec{s} = 0 \quad 2.5$$

$$\int_a^b \vec{V} \cdot d\vec{s} + \int_b^c \vec{V} \cdot d\vec{s} + \int_c^d \vec{V} \cdot d\vec{s} + \int_d^a \vec{V} \cdot d\vec{s} = 0 \quad 2.6$$

However,

$$\int_b^c \vec{V} \cdot d\vec{s} + \int_d^a \vec{V} \cdot d\vec{s} = 0 \quad 2.7$$



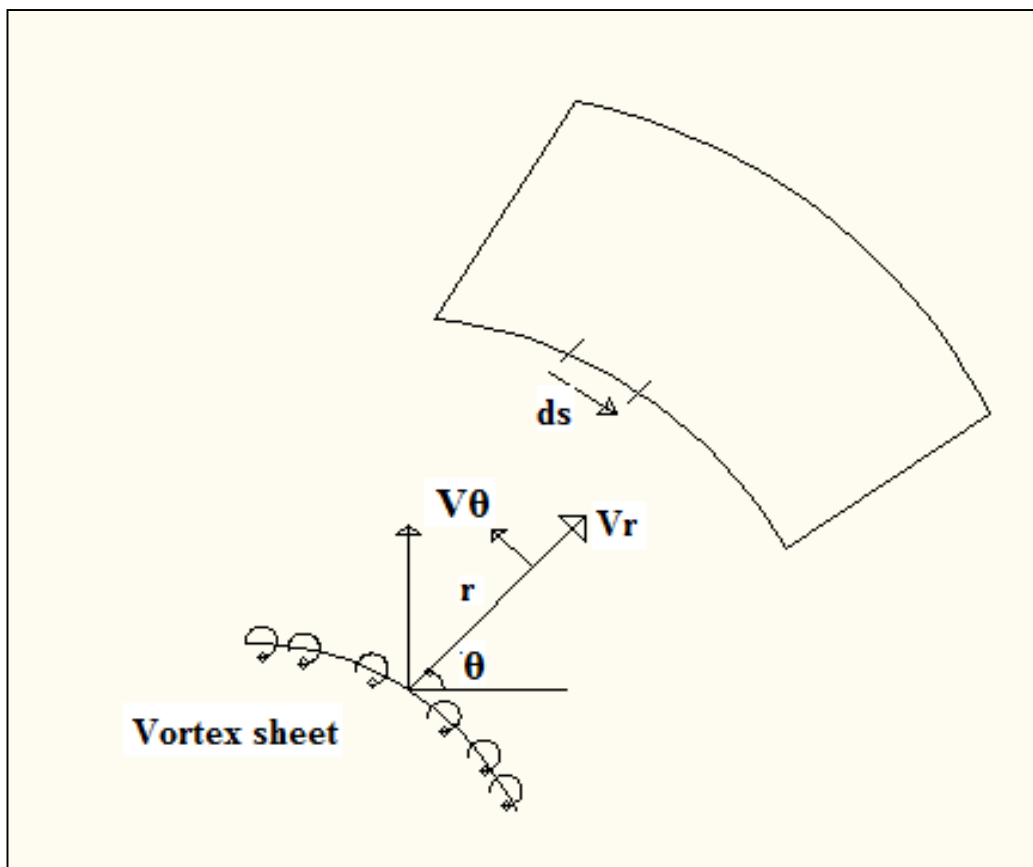
As it constitutes the integral across the slit. Thus,

$$\int_b^c \vec{V} d\vec{s} = - \int_d^a \vec{V} d\vec{s} = \int_d^c \vec{V} d\vec{s} = \Gamma \quad 2.8$$

A vortex filament cannot end in a fluid; it must extend to the boundaries of the fluid or form a closed path. In the absence of rotational external force, if the circulation around a path enclosing a definite group of particles is initially zero, it will remain zero and in the absence of rotational external force, the circulation around a path that encloses a tagged group of elements is invariant. [7]

2.5 Vortex Sheet or vortex surface

An infinite number of straight vortex filaments placed side by side form a vortex sheet. Each vortex filament has an infinitesimal strength $k(s)$.



Where

$k(s)$: is the strength of vortex sheet per unit length along s . And

$$V_{\theta} = \frac{\Gamma}{2\pi r} \text{ for 2 - D (point Vortex)} \quad 2.9$$

A small portion of the vortex sheet of strength $k ds$ induces an infinitesimally small velocity dV at a field point $P(r; \theta)$. So

$$V_{\theta}(\text{vortex filament}) = -\frac{k ds}{2\pi r} \quad 2.10$$

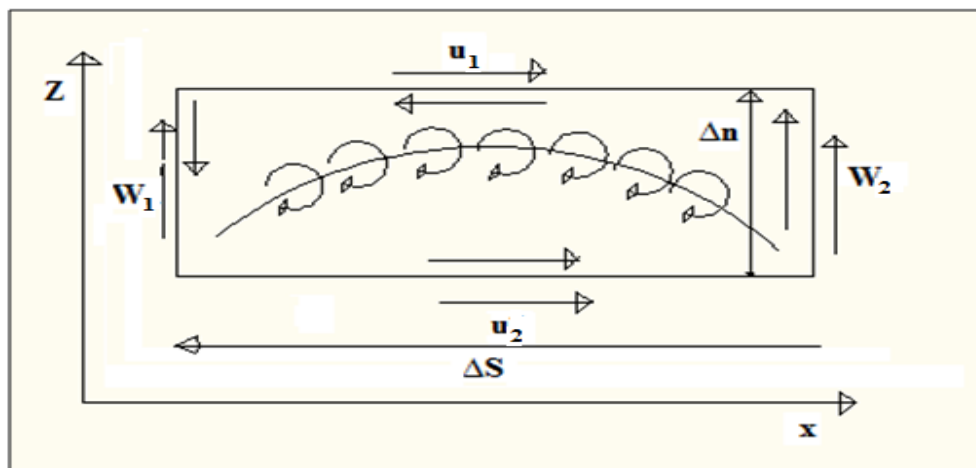
$$\therefore dV_p = -\frac{k ds}{2\pi r} \quad 2.11$$

Circulation Γ around a point vortex is equal to the strength of the vortex. Similarly, the circulation around the vortex sheet is the sum of the strengths of the elemental vortices. Therefore, the circulation Γ for a finite length from point 'a' to point 'b' on the vortex sheet is given by:

$$\Gamma = \int_a^b k(s) ds \quad 2.12$$

Across a vortex sheet, there is a discontinuous change in the tangential component of velocity and the normal component of velocity is preserved.

Here is diagram of an airfoil moving through a fluid at speed U . if we look at the rectangular path around this foil which is " Δn " units high and " ΔS " units long. By multiplying the speed of particles at each point around the rectangle and adding this up as shown in Eq. 2.13.



$$\Delta\Gamma = - \int \vec{V}d\vec{l} = - \int_{\text{BOX}} \vec{V}d\vec{l} = -[w_2\Delta n - u_1\Delta s - w_1\Delta n + u_2\Delta s] \quad 2.13$$

$$k\Delta s = (u_1 - u_2)\Delta s + (w_1 - w_2)\Delta n \quad 2.14$$

As $\Delta n \rightarrow 0$ we get

$$k\Delta s = (u_1 - u_2)\Delta s \text{ or } \gamma = (u_1 - u_2) \quad 2.15$$

$k = (u_1 - u_2)$ states that the local jump in tangential velocity across the vortex sheet is equal to the local sheet strength. [7]

2.5.1 Kutta Condition

The Kutta condition is a principle in steady flow fluid dynamics, especially aerodynamics, which is applicable to solid bodies which have sharp corners such as the trailing edges of airfoils. A body with a sharp trailing edge which is moving through a fluid will create about itself a circulation of sufficient strength to hold the rear stagnation point at the trailing edge. In fluid flow around a body with a sharp corner the Kutta condition refers to the flow pattern in which fluid approaches the corner from both directions, meets at the corner, and then flows away from the body. None of the fluid flows around the corner and remains attached to the body.

When a smooth symmetric body, such as a cylinder with oval cross-section, moves with zero angle of attack through a fluid it generates no lift. There are two stagnation points on the body one at the front and the other at the back. If the oval cylinder moves with a non-zero angle of attack through the fluid there are still two stagnation points on the body - one on the underside of the cylinder, near the front edge; and the other on the topside of the cylinder, near the back edge. The circulation around this smooth cylinder is zero and no lift is generated, despite the positive angle of attack. If an airfoil with a sharp trailing edge as shown in figure 2.3 begins to move with a positive angle of attack through air, the two stagnation points are initially located on the underside near the leading edge and on the topside near the trailing edge, just as with the cylinder. As the air passing the underside of the airfoil reaches the trailing edge it must flow around the trailing edge and along the topside of the airfoil toward the stagnation point on the topside of the airfoil. Vortex flow occurs at the trailing edge and, because the radius of the sharp trailing edge is zero, the speed of the air around the trailing edge should be infinitely fast! Real

fluids cannot move at infinite speed but they can move very fast. The very fast airspeed around the trailing edge causes strong viscous forces to act on the air adjacent to the trailing edge of the airfoil and the result is that a strong vortex accumulates on the topside of the airfoil, near the trailing edge. As the airfoil begins to move it carries this vortex, known as the starting vortex, along with it. The vorticity in the starting vortex is matched by the vorticity in the bound vortex in the airfoil. As the vorticity in the starting vortex progressively increases the vorticity in the bound vortex also progressively increases and causes the flow over the topside of the airfoil to increase in speed. The stagnation point on the topside of the airfoil moves progressively towards the trailing edge. After the airfoil has moved only a short distance through the air the stagnation point on the topside reaches the trailing edge and the starting vortex is cast off the airfoil and is left behind, spinning in the air where the airfoil left it. The starting vortex quickly dissipates due to viscous forces. As the airfoil continues on its way, there is a stagnation point at the trailing edge. The flow over the topside conforms to the upper surface of the airfoil. The flow over both the topside and the underside join up at the trailing edge and leave the airfoil travelling parallel to one another. This is known as the Kutta condition. When an airfoil is moving with a positive angle of attack, the starting vortex has been cast off and the Kutta condition has become established, there is a finite circulation of the air around the airfoil. The airfoil is generating lift, and the magnitude of the lift is given by the Kutta–Joukowski theorem. Whenever the speed or angle of attack of an airfoil changes there is a weak starting vortex which begins to form, either above or below the trailing edge. This a weak starting vortex causes the Kutta condition to be re-established for the new speed or angle of attack. As a result, the circulation around the airfoil changes and so too does the lift in response to the changed speed or angle of attack. [8]

For a given airfoil at a given angle of attack, the value of Γ around the airfoil is such that the flow leaves the trailing edge smoothly.

The Kutta condition tells us how to find Γ ; it is based on experimental observation. A body with finite angle trailing edge (TE) in relative motion through a fluid will create about itself a circulation of sufficient strength to hold the rear stagnation point at the TE. If the TE has a zero angle, the Kutta Condition requires that the velocity of fluid leaving upper and lower surfaces at the TE be equal and non-zero. A body with a finite TE angle will have crossing streamlines at

the TE unless the TE is a stagnation point. The Kutta Condition eliminates the crossing streamlines. Consider the TE as a vortex sheet:

$$k(\text{TE}) = V_u - V_l \quad 2.16$$

If the TE has a finite angle $V_u = V_l = 0$ because TE is a stagnation point. [6]

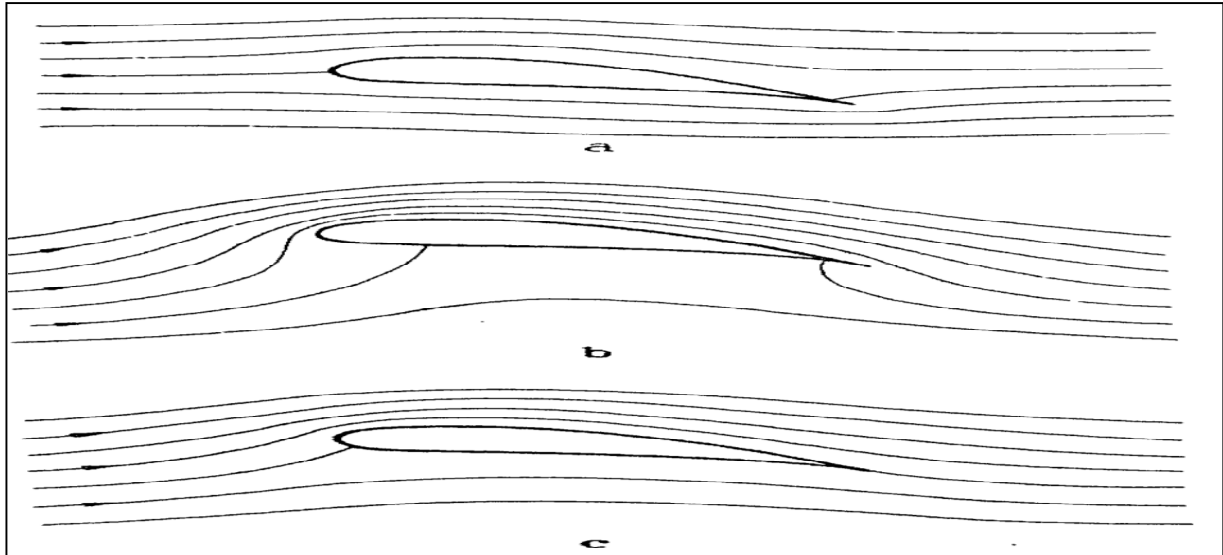


Figure 2.3 Flow around an airfoil for various values of circulation, (a) Circulation $r=0$: rear stagnation point on upper surface. (b) Very large circulation: rear stagnation point on lower surface. (c) Circulation just sufficient to put rear stagnation point on trailing edge. Smooth flow-off: Kutta condition satisfied [6]

2.5.2 Inclined Flat Plate

The simplest case of a lifting-airfoil profile is the inclined flat plate. The angle between the direction of the incident flow and the direction of the plate is called angle of attack of the plate. The flow about the inclined flat plate is obtained as shown in figure 2.4 by superposition of the plate in parallel flow (a) and the plate in normal flow (b). The resulting flow

$$(c) = (a) + (b) \quad 2.17$$

does not yet produce lift on the plate because identical flow conditions exist at the leading and trailing edges. The front stagnation point is located on the lower surface and the rear stagnation point on the upper surface of the plate. [6]

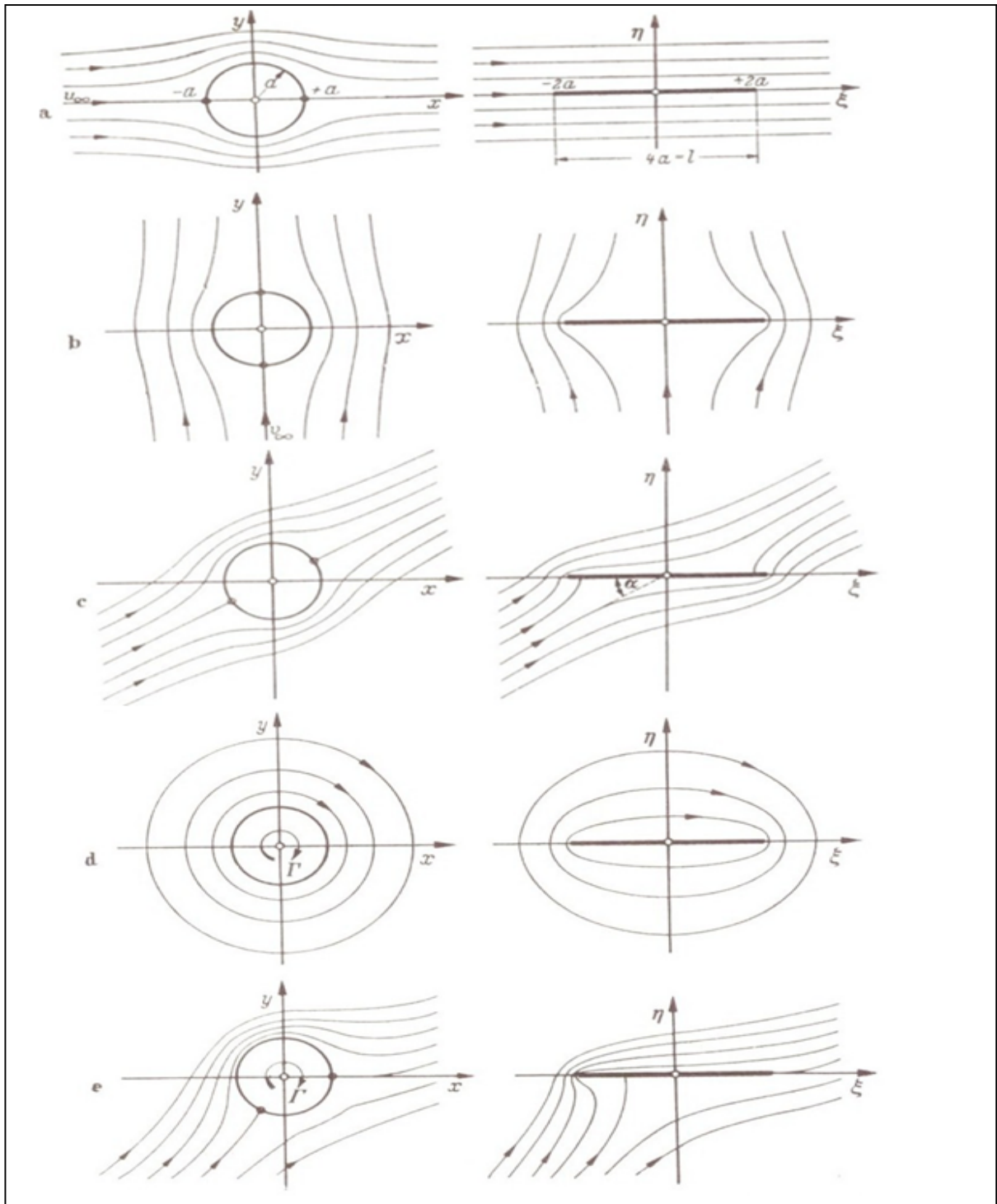


Figure 2.4 Flow about an inclined flat plate, (a) Flat plate in parallel flow, (b) Flat plate in normal (stagnation) flow, (c) Inclined flat plate without lift, (c) = (a) + (b). (d) Pure circulation flow. (e) Inclined flat plate with lift (Kutta condition), (e) = (c) + (d). [6]

To establish a plate flow with lift, a circulation Γ according to Fig. 2.4d must be superimposed on (c). The resulting flow

$$(e) = (c) + (d) = (a) + (b) + (d) \quad 2.18$$

is the plate flow with lift. The magnitude of the circulation is determined by the condition of smooth flow-off at the plate trailing edge; for example, the rear stagnation point lies on the plate trailing edge (Kutta condition). By superposition of the three flow fields, a flow is obtained around the circle of radius a with its center at $z = 0$. It is approached by the flow under the angle α with the x axis, α being $\arctan (v_\infty/u_\infty)$. The complex stream function of this flow

$$F(z) = u_\infty \left(Z + \frac{a^2}{Z} \right) \quad \text{and } Z = x + yi \quad 2.19$$

Where,

Z : complex argument

a : Radius of circular cylinder.

For an irrotational flow around the coordinate origin, that is, for a plane potential vortex, the stream function is

$$F(z) = \frac{i\Gamma}{2\pi} \ln Z \quad 2.20$$

Where Γ is a clockwise-turning circulation.

The complex stream function of this flow

$$F(z) = (u_\infty - iv_\infty)z + (u_\infty + iv_\infty) \frac{a^2}{Z} + \frac{i\Gamma}{2\pi} \ln Z \quad 2.21$$

For the mapping, the Joukowski transformation function

$$\zeta = f(z) = Z + \frac{a^2}{Z} \quad 2.22$$

This function transforms the circle of radius a in the z plane into the plate of length $c=4a$ in the ζ plane.

$$\bar{w}(\zeta) = \frac{dF}{d\zeta} = \frac{dF}{dz} \frac{dz}{d\zeta} = \bar{w}(z) \frac{dz}{d\zeta} \quad 2.23$$

Where

$\bar{w}(z)$: Stream function

The velocity distribution about the plate is obtained with the help of Eq. 2.23 of the velocity field of the body after some auxiliary calculations as

$$\bar{w}(\zeta) = u_{\infty} \mp i \frac{v_{\infty} \zeta - \frac{\Gamma}{2\pi}}{\sqrt{\zeta^2 - 4a^2}} \quad 2.24$$

The magnitude of the circulation Γ is now to be determined from the Kutta condition. Smooth flow-off (outflow) at the trailing edge requires that is, at $\zeta = +2a$ - the velocity remains finite. Therefore, the nominator of the fraction in Eq. 2.24 must vanish for $\zeta = 2a$. Hence, because of $4a = c$,

$$\Gamma = 4\pi a v_{\infty} = \pi c v_{\infty} \quad 2.25$$

and the velocity distribution on the plate itself becomes, with $\zeta = \xi$ and $|\xi| < c/2$,

$$u = w_{\infty} \left(\cos\alpha \pm \sin\alpha \sqrt{\frac{c - 2\xi}{c + 2\xi}} \right) \quad 2.26$$

The + sign applies to the upper surface, the - sign to the lower surface. With w_{∞} the resultant of the incident flow, and α , the angle of attack between plate and incident flow resultant, the flow components are given by $u_{\infty} = w_{\infty} \cos \alpha$ and $v_{\infty} = w_{\infty} \sin \alpha$.

At the plate leading edge, i.e. $\xi = -c/2$, the velocity is infinitely high. The flow around the plate comes from below, as seen from figure 2.4e. On the plate trailing edge, $\xi = +c/2$, the tangential velocity has the value $u = v_{\infty} \cos \alpha$. At an arbitrary station of the plate, the tangential velocities on the lower and upper surfaces have a difference in magnitude $\Delta u = u_u - u_h$. At the trailing edge, $\Delta u = 0$ (smooth flow-off). [6]

2.6 Flat Plate at an Angle of Attack

Velocity induced by a 2-D vortex as shown in figure 2.5 is $\vec{V} = v_\theta \hat{e}_\theta = -\frac{\Gamma}{2\pi r}$ where Γ is the strength of the 2-D vortex. Similarly the velocity induced by the vortex sheet of infinitesimal length ds is given by

$$d\vec{v}_p = -\frac{k(s)ds}{2\pi r} \hat{e}_\theta \quad 2.27$$

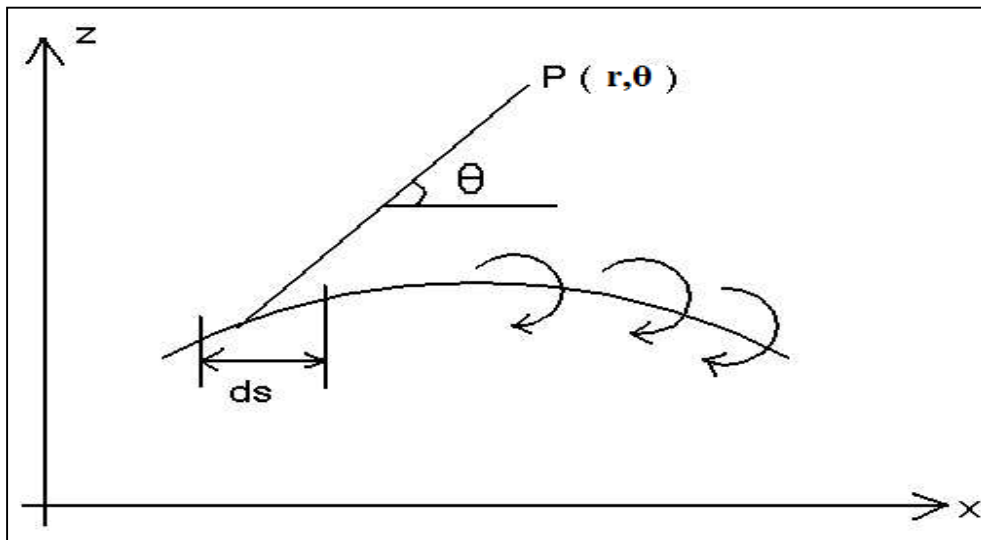


Figure 2.5 Velocity induced by a 2-D vortex [7]

To force the mean camber line to be a streamline, the sum of all velocity components normal to the mean camber line must be equal to zero. Consider the flow induced by elemental vortex sheet ds at a point P on the vortex sheet. It is perpendicular to the line connecting the center of ds to the point P see figure 2.6 given by

$$d\vec{v}_p = -\frac{k(s)ds}{2\pi r} \hat{e}_\theta \quad 2.28$$

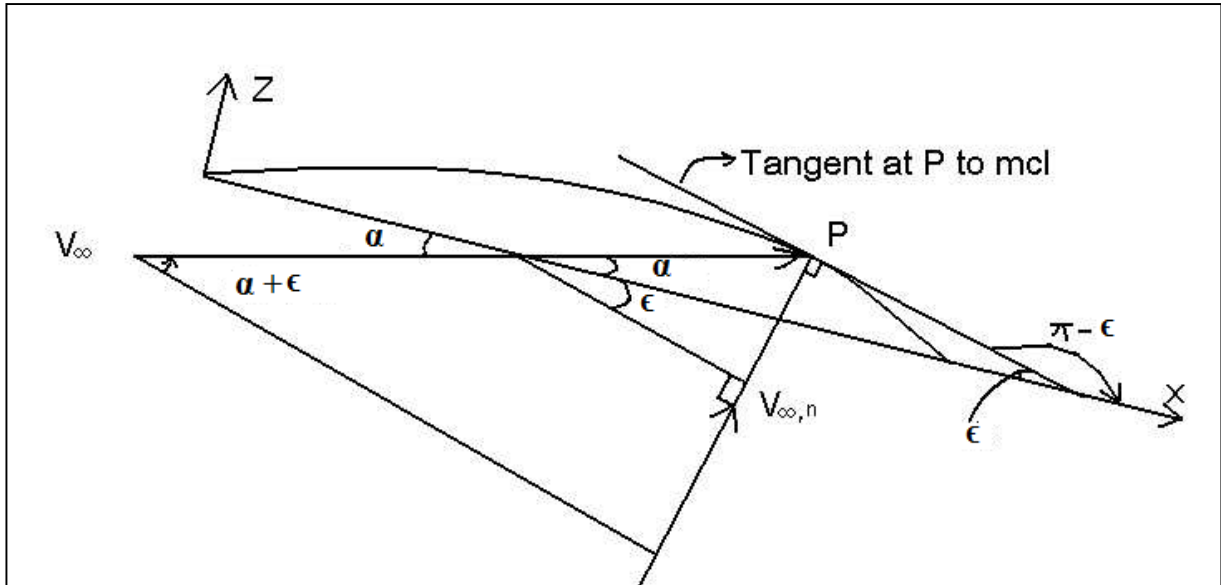


Figure 2.6 Forces in vortex sheet [7]

Thus dw'_p the velocity normal to the mean camber line is:

$$dw'_p = dv_p \cos \beta = -\frac{k(s) \cos \beta}{2\pi r} ds \quad 2.29$$

Where β is the angle made by dv_p to the normal at P, and r is the distance from the center of ds to the point P.

The induced velocity due to the vortex sheet representing the entire mean camber line is given by;

$$dw'_p = -\frac{1}{2\pi r} \int_{LE}^{TE} k(s) \cos \beta ds \quad 2.30$$

Now determine the component of the free stream velocity normal to the mean camber line.

$$V_{\infty,n} = V_{\infty} \sin(\alpha + \epsilon) \quad 2.31$$

Where α is the angle of attack and ϵ is the angle made by the tangent at point P to the x-axis.

The slope of the tangent line at point P is given by:

$$\frac{dz}{dx} = \tan(\pi - \epsilon) = -\tan\epsilon \quad 2.32$$

$$\epsilon = \tan^{-1}\left(-\frac{dz}{dx}\right) \quad 2.33$$

$$V_{\infty,n} = V_{\infty} \sin\left(\alpha + \tan^{-1}\left(-\frac{dz}{dx}\right)\right) \quad 2.34$$

In order that the mean camber line is a streamline

$$w'_p(s) + V_{\infty,n} = 0 \text{ or } -\frac{1}{2\pi r} \int_{LE}^{TE} k(s) \cos\beta ds + V_{\infty} \sin\left(\alpha + \tan^{-1}\left(-\frac{dz}{dx}\right)\right) = 0 \quad 2.35$$

Within thin airfoil theory approximation $s \rightarrow x$, $ds \rightarrow dx$, $\cos\beta = 1$ and $r \rightarrow (x_0 - x)$, where x varies from 0 to c , and x_0 refers to the point P.

After changing these variables and making the small angle approximation for sin and tan, and upon rearrangement we get:

$$\frac{1}{2\pi} \int_0^c \frac{\gamma(X)}{(X_0 - X)} dX = V_{\infty} \left(\alpha - \frac{dz}{dx}\right) \quad 2.36$$

The following analysis is an exact solution to the flat plate or an approximate solution to the symmetric airfoil. The mean camber line becomes the chord and hence:

$$\frac{dZ}{dX} = 0 \quad 2.37$$

$$\frac{1}{2\pi} \int_0^c \frac{\gamma(X)}{(X_0 - X)} dX = V_{\infty} \alpha \quad 2.38$$

In order to facilitate analytic solution, we do a variable transformation such that:

$$X = \frac{c}{2}(1 - \cos\theta) \quad 2.39$$

And

$$X_0 = \frac{c}{2}(1 - \cos\theta_0) \quad 2.40$$

$\theta = 0$ at Leading edge (LE) and $\theta = \pi$ at TE and θ increases in clock wise (CW),

$$dx = (c/2) \sin\theta d\theta$$

$$\frac{1}{2\pi} \int_0^c \frac{k(X)(c/2)\sin\theta}{\frac{c}{2}\left((1 - \cos\theta_0) - \frac{c}{2}(1 - \cos\theta)\right)} d\theta = V_{\infty} \alpha \quad 2.41$$

$$\frac{1}{2\pi} \int_0^\pi \frac{k(X)\sin\theta}{(\cos\theta - \cos\theta_0)} d\theta = V_\infty \alpha \quad 2.42$$

Here we simply state a rigorous solution for $k(\theta)$ as:

$$\gamma(\theta) = 2\alpha V_\infty \frac{1 + \cos\theta}{\sin\theta} \quad 2.43$$

We can verify this solution by substitution as follows:

$$\frac{1}{2\pi} \int_0^\pi \frac{k(X)\sin\theta}{(\cos\theta - \cos\theta_0)} d\theta = \frac{V_\infty \alpha}{\pi} \int_0^\pi \frac{1 + \cos\theta}{(\cos\theta - \cos\theta_0)} d\theta \quad 2.44$$

We now use the following result to evaluate the above integral.

$$\begin{aligned} \frac{V_\infty \alpha}{\pi} \int_0^\pi \frac{1 + \cos\theta}{(\cos\theta - \cos\theta_0)} d\theta \\ = \frac{V_\infty \alpha}{\pi} \int_0^\pi \frac{1}{(\cos\theta - \cos\theta_0)} d\theta + \frac{V_\infty \alpha}{\pi} \int_0^\pi \frac{\cos\theta}{(\cos\theta - \cos\theta_0)} d\theta \end{aligned} \quad 2.45$$

$$\frac{V_\infty \alpha}{\pi} (0 + \pi) = V_\infty \alpha \quad 2.46$$

Thus, it satisfies the equation:

$$\frac{1}{2\pi} \int_0^\pi \frac{k(X)\sin\theta}{(\cos\theta - \cos\theta_0)} d\theta = V_\infty \alpha \quad 2.47$$

In addition, the solution for γ also satisfies the Kutta condition.

When $\theta = \pi$,

$$k(\pi) = 2V_\infty \alpha \frac{1 - 1}{0} \quad 2.48$$

By using L'Hospital' rule, we get

$$k(\pi) = 2V_\infty \alpha \frac{-\sin\pi}{\cos\pi} = 0 \quad 2.49$$

Thus it satisfies the Kutta condition. [7]

2.7 Aerodynamic Force

Aerodynamic force as shown in figure 2.7 is the resultant force exerted on a body by the air (or some other gas) in which the body is immersed, and is due to the relative motion between the body and the fluid. An aerodynamic force arises from two causes: The force due to the pressure on the surface of the body and the force due to viscosity, also known as skin friction. When a body is exposed to the wind it experiences a force in the direction in which the wind is moving.

This is an aerodynamic force. When a body is moving in air or some other gas the aerodynamic force is usually called drag.

When an airfoil or a wing or a glider is moving relative to the air it generates an aerodynamic force that is partly parallel to the direction of relative motion, and partly perpendicular to the direction of relative motion. This aerodynamic force is commonly resolved into two components: Drag is the component parallel to the direction of relative motion, and lift is the component perpendicular to the direction of relative motion. The force created by a propeller or a jet engine is called thrust and it is also an aerodynamic force. The aerodynamic force on a powered airplane is commonly resolved into three components thrust, lift and drag, the only other force acting on a glider or powered airplane is its weight (Weight is a body force, not an aerodynamic force).

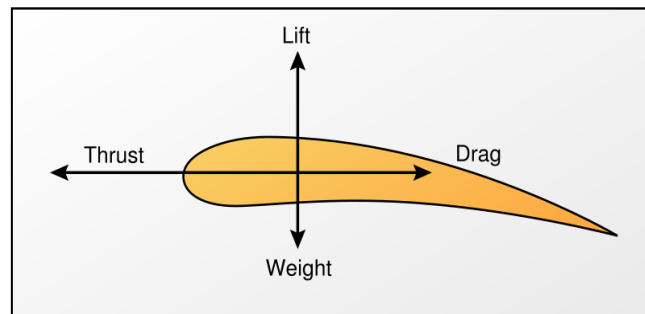


Figure 2.7 Forces on airfoil. [9]

2.7.1 Lift and Drag Force on Airfoil

A fluid flowing past the surface of a body exerts a surface force on it. Lift is defined to be the component of this force that is perpendicular to the oncoming flow direction. It contrasts with the drag force, which is defined to be the component of the surface force parallel to the flow direction.

The equations for calculating lift and drag are very similar. The lift that an airfoil generates depends on the density of the air, the velocity of the airflow, the viscosity and compressibility of the air, the surface area of the airfoil, the shape of the airfoil, and the angle of the airfoil's angle of attack. However, dependence on the airfoil's shape, the angle of attack, air viscosity and compressibility are very complex. Thus, they are characterized by a single variable in the lift

equation, called the lift coefficient. Due to the complexities of the lift coefficient, it is generally found via experimentation in a wind tunnel where the remaining variables can be controlled. Therefore, the lift equation is given by:

$$L = \frac{1}{2} U_{\infty}^2 \rho C_L A \quad 2.50$$

Where L is the lifting force, ρ is the density of air, U_{∞} is the relative velocity of the airflow A is the area of the airfoil as viewed from an overhead perspective, and C_L is the lift Coefficient.

As with lift, the drag of an airfoil depends on the density of the air, the velocity of the airflow, the viscosity and compressibility of the air, the surface area of the airfoil, the shape of the airfoil, and the angle of attack.

The complexities associated with drag and the airfoil's shape, angle of attack, the air's viscosity, and air's compressibility are simplified in the drag equation by use of the drag coefficient. The drag coefficient is generally found through testing in a wind tunnel, where the drag can be measured, and the drag coefficient is calculated by rearranging the drag equation

$$D = \frac{1}{2} U_{\infty}^2 \rho C_D A \quad 2.51$$

In the drag equation, D is the drag force, ρ is the density of the air, U_{∞} is the velocity of the air, A is a reference area, and C_D is the drag Coefficient. [10]

The drag force is the net exerted by a fluid on a body in the direction of flow due to the combined effects of wall shear and pressure forces.

The part of drag that is due directly to wall shear stress is called the skin friction drag or just friction drag since it is caused by frictional effects, and the part that is due directly to pressure is called the pressure drag or called the form drag because of its strong dependence on the form or shape of the body.

2.7.2 Drag Coefficient

In fluid dynamics, the drag coefficient (commonly denoted as: C_D or C_w) is a dimensionless quantity that is used to quantify the drag or resistance of an object in a fluid environment such as air or water. It is used in the drag equation, where a lower drag coefficient indicates the object will have less aerodynamic or hydrodynamic drag. The drag coefficient is always associated with a particular surface area. The drag coefficient of any object comprises the effects of the two basic

contributors to fluid dynamic drag: skin friction and form drag. The drag coefficient of a lifting airfoil or hydrofoil also includes the effects of lift-induced drag. The drag coefficient of a complete structure such as an aircraft also includes the effects of interference drag

The drag coefficient C_D is defined as:

$$C_D = \frac{2D}{\rho U_\infty^2 A} \quad 2.53a$$

Where,

D is the drag force, which is by definition the force component in the direction of the flow velocity,

ρ is the mass density of the fluid,

V_∞ is the speed of the object relative to the fluid, and

A is the reference area. [11]

Drag on airfoils arises from viscous and pressure forces. Viscous drag or Skin friction changes with Reynolds number and arises from the interaction between the fluid and the skin of the body but only slightly with angle of attack. These relationships and some commonly used terminology are illustrated in figure 2.8.

A useful approximation to drag polar for complete aircraft may be obtained by adding the induced drag or vortex drag, or sometimes drag due to lift, is a drag force that occurs whenever a moving object redirects the airflow coming at it to the drag at zero lift. The drag at any lift coefficient is obtained from

$$C_D = C_{D,0} + C_{D,i} = C_{D,0} + \frac{C_L^2}{\pi ar} \quad , \quad ar = \frac{b^2}{A_p} \quad 2.53b$$

Where,

$C_{D,0}$: drag coefficient at zero lift

$C_{D,i}$: induced drag coefficient

ar: Aspect ratio

b: wingspan or is the distance from one wingtip to the other wingtip of the airplane

A_p : Planform area

c: chord length. [12]

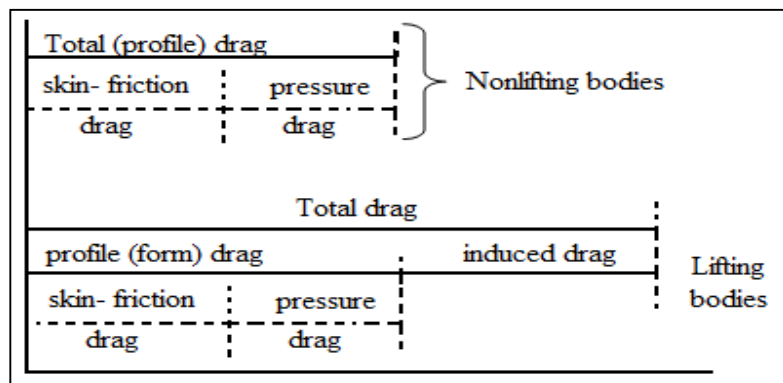


Figure 2.8 Drag breakdowns on nonlifting and lifting bodies [12]

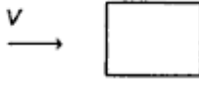
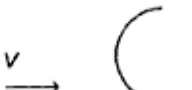
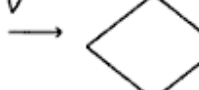
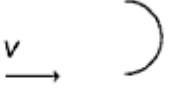
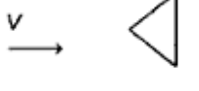
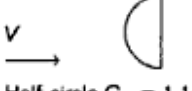
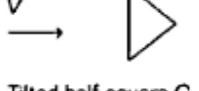
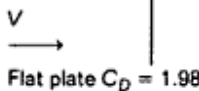
The drag coefficient for all objects with sharp edge is essentially independent of Reynolds number (for $Re \geq 10000$) because the separation points and therefore the size of the wake are fixed by geometry of the object. Drag coefficients for selected objects are given in table 2.1

The friction coefficient for laminar flow over a flat plate can be determined theoretically by solving the conservation of mass and momentum equations numerically. For turbulent flow, however, it must be determined experimentally and expressed by empirical correlation. The local friction coefficient varies along the surface of the flat plate as a result of the changes in the velocity boundary layer in flow direction. We are usually interested in drag force on the entire surface, which can be determined using average friction coefficient. The average friction coefficient over the entire plate is determined by

$$\text{Laminar, } C_f = \frac{1.33}{Re_L^{1/2}} \quad Re < 5 \times 10^5 \quad ,$$

$$\text{turbulent, } C_f = \frac{0.074}{Re_L^{1/5}} \quad 5 \times 10^5 < Re < 10^7 \quad 2.53c$$

Table 2.1 Drag coefficient data for selected objects ($Re \geq 10^4$). [13]

 Circle $C_D = 1.17$	 Square $C_D = 2.05$
 Semicircular cylinder $C_D = 1.20$	 Tilted square $C_D = 1.55$
 Half-circular cylinder $C_D = 2.30$	 Tilted half-square $C_D = 1.55$
 Half-circle $C_D = 1.16$	 Tilted half-square $C_D = 2.00$
	 Flat plate $C_D = 1.98$

2.7.3 Lift Coefficient

The lift coefficient (C_L , C_a) is a dimensionless coefficient that relates the lift generated by an aerodynamic body such as a wing or complete aircraft, the dynamic pressure of the fluid flow around the body, and a reference area associated with the body. It is also used to refer to the aerodynamic lift characteristics of a 2D airfoil section. Lift coefficient may be used to relate the total lift generated by an aircraft to the total area of the wing of the aircraft. In this application it is called the aircraft or plan form lift coefficient C_L .

The lift coefficient C_L is equal to:

$$C_L = \frac{L}{\frac{1}{2}\rho U_\infty^2 A} = \frac{2L}{\rho U_\infty^2 A} = \frac{L}{qA} \quad 2.54$$

Where

- L is the lift force,
- ρ is fluid density,

- q is dynamic pressure, and
- A is plan form area.

Lift coefficient may also be used as a characteristic of a particular shape (or cross-section) of an airfoil. In this application it is called the section lift coefficient C_L . It is common to show, for a particular airfoil section, the relationship between section lift coefficient and angle of attack. It is also useful to show the relationship between section lift coefficients and drag coefficient.

The section lift coefficient is based on the concept of an infinite wing of non-varying cross-section, the lift of which is bereft of any three-dimensional effects - in other words the lift on a 2D section. It is not relevant to define the section lift coefficient in terms of total lift and total area because they are infinitely large. Rather, the lift is defined per unit span of the wing L . In such a situation, the above formula becomes:

$$C_L = \frac{L}{\frac{1}{2}\rho U_\infty^2 c} \quad 2.55$$

Where c is the chord length of the airfoil. The section lift coefficient for a given angle of attack can be approximated using, for example, the Theory, or determined from wind tunnel tests on a finite-length test piece, with end-plates designed to ameliorate the 3D effects associated with the trailing vortex wake structure.

Note that the lift equation does not include terms for angle of attack that is because the mathematical relationship between lift and angle of attack varies greatly between airfoils and is, therefore, not constant. (In contrast, there is a straight-line relationship between lift and dynamic pressure; and between lift and area.) The relationship between the lift coefficient and angle of attack is complex and can only be determined by experimentation or complex analysis. See the accompanying graph. The graph for section lift coefficient vs. angle of attack follows the same general shape for all airfoils, but the particular numbers will vary. The graph shows an almost linear increase in lift coefficient with increasing angle of attack, up to a maximum point, after which the lift coefficient reduces. The angle at which maximum lift coefficient occurs is the stall angle of the airfoil. [14]

2.7.4 Kutta-Joukowski Lift Theorem

Treatment of the theory of lift of a body in a fluid flow is considerably less difficult than that of drag because the theory of drag requires incorporation of the viscosity of the fluid. The lift, however, can be obtained in very good approximation from the theory of inviscid flow. The following discussions may be based, therefore, on in viscid, incompressible flow. For treatment of the problem of plane (two-dimensional) flow about an airfoil, it is assumed that the lift-producing body is a very long cylinder (theoretically of infinite length) that lies normal to the flow direction. Then, all flow processes are equal in every cross section normal to the generatrix of the cylinder; that is, flow about an airfoil of infinite length is two-dimensional. Particular flow processes that have a marked effect on both lift and drag take place at the wing tips of finite-span wings.

Lift production on an airfoil is closely related to the circulation of its velocity near-field. Let us explain this interrelationship qualitatively. The flow about an airfoil profile with lift is shown in Fig. 2.10. The lift L is the resultant of the pressure forces on the lower and upper surfaces of the contour. Relative to the pressure at large distance from the profile, there is higher pressure on the lower surface, lower pressure on the upper surface. It follows, then, from the Bernoulli equation, that the velocities on the lower and upper surfaces are lower or higher, respectively, than the velocity W_∞ of the incident flow. With these facts in mind, it is easily seen from figure 2.9 that the circulation, taken as the line integral of the velocity along the closed curve K , differs from zero. But also for a curve lying very close to the profile, the circulation is unequal to zero if lift is produced. The velocity field ambient to the profile can be thought to have been produced by a clockwise-turning vortex Γ that is located in the airfoil. This vortex, which apparently is of basic importance for the creation of lift, is called the bound vortex of the wing.

In plane flow, the quantitative interrelation of lift L , incident flow velocity W_∞ , and circulation Γ is given by the Kutta-Joukowski equation. Its simplified derivation, which will now be given, is not quite correct but has the virtue of being particularly plain. Let us cut out of the infinitely long airfoil a section of width b (Figure 2.10), and of this a strip of depth dx parallel to the leading edge. This strip of plan form area $dA = b dx$ is subject to a lift

$dL = (p_L - p_u) dA$ because of the pressure difference between the lower and upper surfaces of the airfoil. The vector dL can be assumed to be normal to the direction of incident flow if the small angles are neglected that are formed between the surface elements and the incident flow direction.

The pressure difference between the lower and upper surfaces of the airfoil can be expressed through the velocities on the lower and upper surfaces by applying the Bernoulli equation. [6]

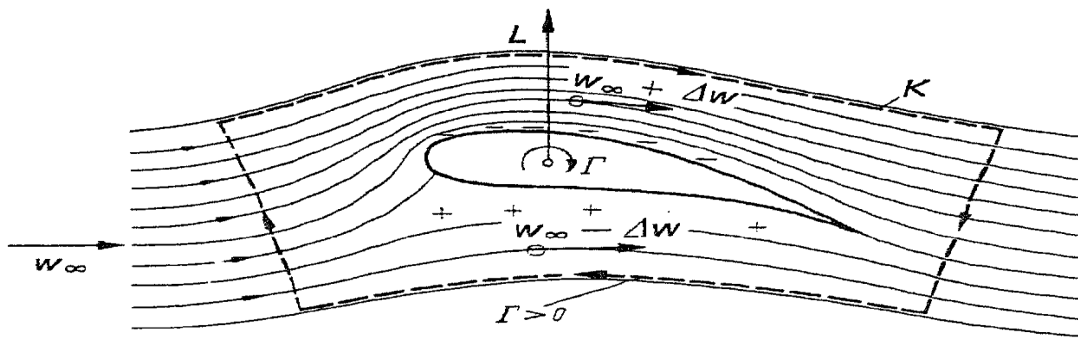


Figure 2.9 Flow around an airfoil profile with lift L , Γ = circulation of the airfoil. [6]

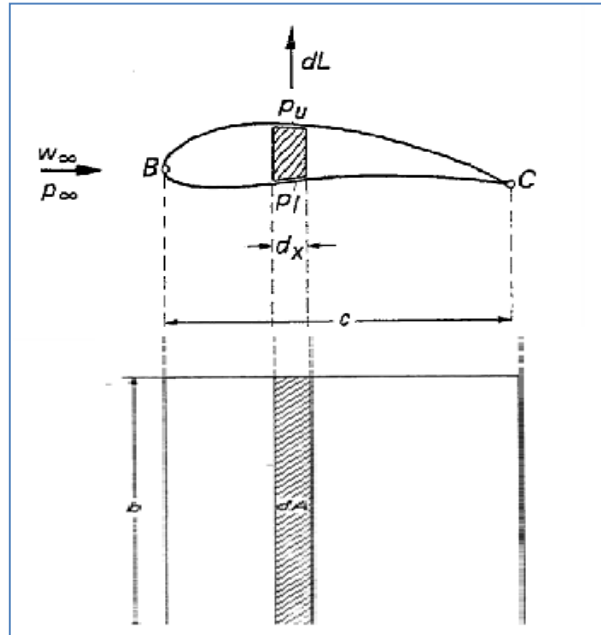


Figure 2.10 Notations for the computation of lift from the pressure distribution on the airfoil. [6]

From Figure 2.8, the velocities on the upper and lower surfaces of the airfoil are $(W_\infty + \Delta W)$ and $(W_\infty - \Delta W)$, respectively. The Bernoulli equation then furnishes for the pressure difference

$$P_L - P_u = \frac{\rho}{2}(W_\infty + \Delta W)^2 - \frac{\rho}{2}(W_\infty - \Delta W)^2 = 2\rho W_\infty \Delta W \quad 2.56$$

Where the assumption has been made that the magnitudes of the circulatory velocities on the lower and upper surfaces are equal,

$$|\Delta W|_L = |\Delta W|_U = |\Delta W| \quad 2.57$$

By integration, the total lift of the airfoil is consequently obtained as

$$L = \int_{(A)} \Delta P dA = b \int_B^C \Delta P dx = 2\rho W_\infty \int_B^C \Delta W dx \quad 2.58$$

The integration has been carried from the leading to the trailing edge (length of airfoil chord c).

The circulation along any line \vec{l} around the wing surface is

$$\Gamma = \oint_{(l)} \vec{W} dl \quad 2.59$$

$$\Gamma = \int_{B,u}^C \Delta W dx - \int_{C,l}^B \Delta W dx = 2 \int_B^C \Delta W dx \quad 2.60$$

The first integral in the first equation is to be taken along the upper surface, the second along the lower surface of the wing. From Eq. 2.58 the lift is then given by

$$L = \rho W_\infty \Gamma \quad 2.61$$

This equation was found first by Kutta in 1902 and independently by Joukowski in 1906 and is the exact relation, as can be shown, between lift and circulation. Furthermore, it can be shown that the lift acts normal to the direction of the incident flow. [6]

2.7.5 Magnitude and Formation of Circulation

If the magnitude of the circulation is known, the Kutta-Joukowski formula, Eq. 2.61, is of practical value for the calculation of lift. However, it must be clarified as to what way the circulation is related to the geometry of the wing profile, to the velocity of the incident flow, and to the angle of attack. This interrelation cannot be determined uniquely from theoretical considerations, so it is necessary to look for empirical results.

The technically most important wing profiles have, in general, a more or less sharp trailing edge. Then the magnitude of the circulation can be derived from experience, namely, that there is no flow around the trailing edge, but that the fluid flows off the trailing edge smoothly. This is the important Kutta flow-off condition, often just called the Kutta condition.

For a wing with angle of attack, yet without circulation (see Figure 2-3a), the rear stagnation point, that is, the point at which the streamlines from the upper and lower sides recombine, would lie on the upper surface. Such a flow pattern would be possible only if there were flow around the trailing edge from the lower to the upper surface and, therefore, theoretically (in inviscid flow) an infinitely high velocity at the trailing edge with an infinitely high negative pressure. On the other hand, in the case of a very large circulation (see Fig. 2-10b) the rear stagnation point would be on the lower surface of the wing with flow around the trailing edge from above. Again velocity and negative pressure would be infinitely high.

Experience shows that neither case can be realized; rather, as shown in Figure 2-3c, a circulation forms of the magnitude that is necessary to place the rear stagnation point exactly on the sharp trailing edge. Therefore, no flow around the trailing edge occurs, either from above or from below, and smooth flow-off is established. The condition of smooth flow-off allows unique determination of the magnitude of the circulation for bodies with a sharp trailing edge from the body shape and the inclination of the body relative to the incident flow direction. This statement is valid for the inviscid potential flow. In flow with friction, a certain reduction of the circulation from the value determined for frictionless flow is observed as a result of viscosity effects.

For the formation of circulation around a wing, information is obtained from the conservation law of circulation in frictionless flow (Thomson theorem). This states that the circulation of a fluid-bound line is constant with time. This behavior will be demonstrated on a wing set in

motion from rest, Figure 2-11. Each fluid-bound line enclosing the wing at rest (Figure 2-11a) has a circulation $\Gamma = 0$ and retains, therefore, $\Gamma = 0$ at all later times. Immediately after the beginning of motion, frictionless flow without circulation is established on the wing (as shown in Fig. 2-11a), which passes the sharp trailing edge from below (Figure 2-11 b). Now, because of friction, a left-turning vortex is formed with a certain circulation $-\Gamma$. This vortex quickly drifts away from the wing and represents the so-called starting or initial vortex $-\Gamma$ (Figure 2-11c).

For the originally observed fluid-bound line, the circulation remains zero, even though the line may become longer with the subsequent fluid motion. It continues, however, to encircle the wing and starting vortex. Since the total circulation of this fluid-bound line remains zero for all times according to the Thomson theorem, somewhere within this fluid-bound line a circulation must exist equal in magnitude to the circulation of the starting vortex but of reversed sign. This is the circulation $+\Gamma$ of the wing. The starting vortex remains at the starting location of the wing and is, therefore, sometime after the beginning of the motion sufficiently far away from the wing to be of negligible influence on the further development of the flow field. The circulation established around the wing, which produces the lift, can be replaced by one or several vortices within the wing of total circulation $+\Gamma$ as far as the influence on the ambient flow field is concerned. They are called the bound vortices. From the above discussions it is seen that the viscosity of the fluid, after all, causes the formation of circulation and, therefore, the establishment of lift. In an inviscid fluid, the original flow without circulation and, therefore, with flow around the trailing edge, would continue indefinitely. No starting vortex would form and, consequently, there would be no circulation about the wing and no lift.

Viscosity of the fluid must therefore be taken into consideration temporarily to explain the evolution of lift, that is, the formation of the starting vortex. After establishment of the starting vortex and the circulation about the wing, the calculation of lift can be done from the laws of frictionless flow using the Kutta-Joukowski equation and observing the Kutta condition.

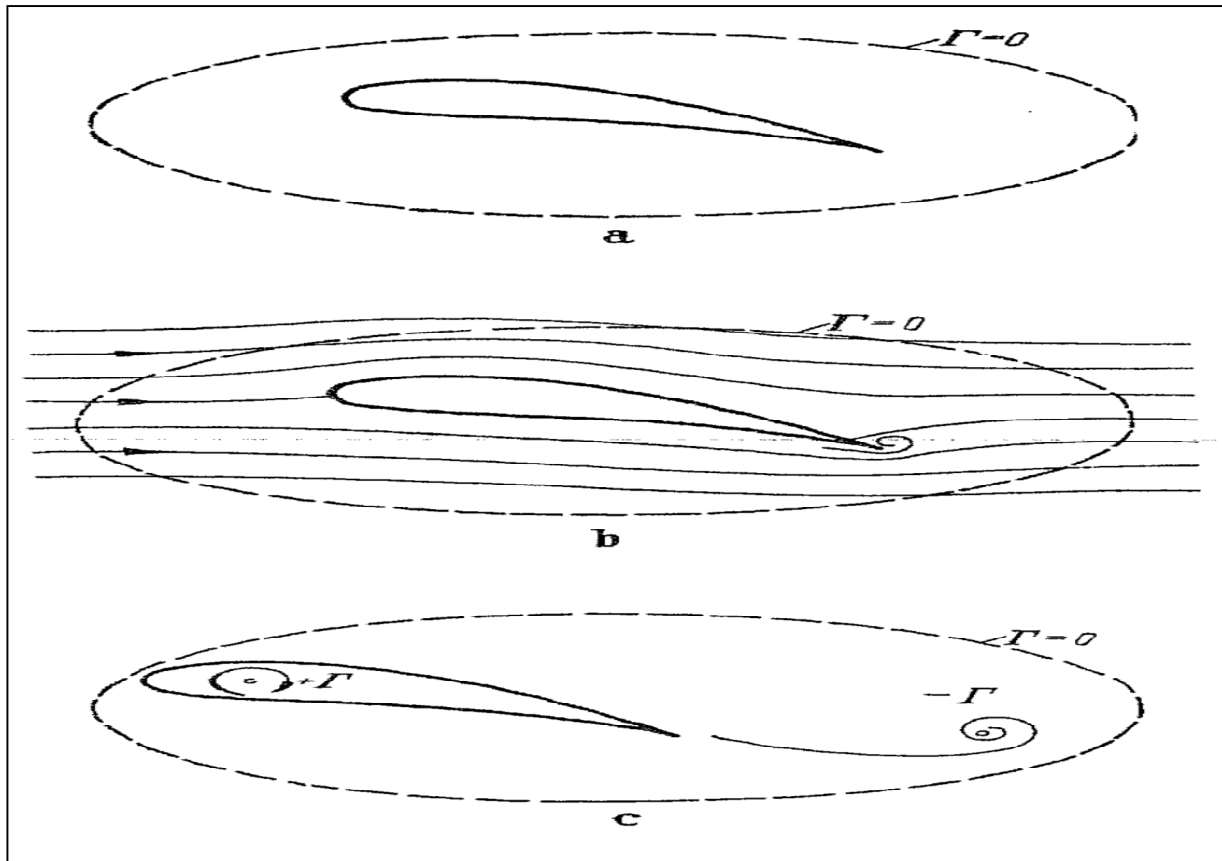


Figure 2.11 Development of circulation during setting in motion of a wing, (a) Wing in stagnant fluid. (b) Wing shortly after beginning of motion; for the liquid line chosen in (a), the circulation $\Gamma = 0$; because of flow around the trailing edge, a vortex forms at this station, (c) This vortex formed by flow around the trailing edge is the so-called starting vortex $-\Gamma$; a circulation $+\Gamma$ develops consequently around the wing. [6]

2.8 Pitching moment

The pitching moment on a wing may be estimated experimentally by two principal methods: direct measurement on a balance, or by pressure plotting, In either case, the pitching moment coefficient is measured about some definite point on the aerofoil chord, while for some particular purpose it may be desirable to know the pitching moment coefficient about some other point on the chord. To convert from one reference point to the other is a simple application of statics.

Suppose, for example, the lift and drag are known, as also is the pitching moment M_a about a point distance a from the leading edge, and it is desired to find the pitching moment M_x about a different point, distance x behind the leading edge. The situation is then as shown in Figure. 2.12. Figure 2.12a represents the known conditions, and Figure 2.12b the unknown conditions. These represent two alternative ways of looking at the same physical system, and must therefore give identical effects on the aerofoil. Obviously, then, $L = L$ and $D = D$. Taking moments in each case about the leading edge:

$$M_{LE} = M_a - Lc\cos\alpha - D\sin\alpha = M_x - Lx\cos\alpha - Dx\sin\alpha \quad 2.62$$

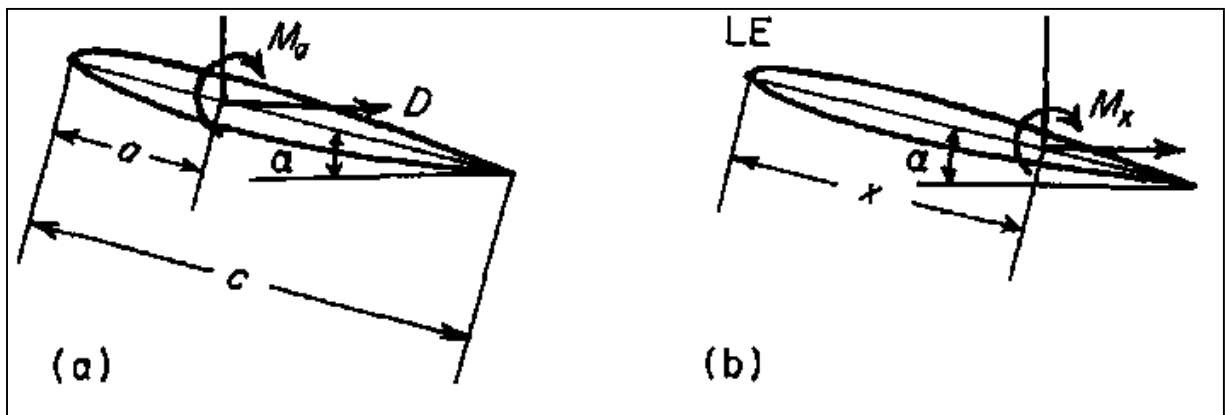


Figure 2.12 pitching moment on a wing [1]

Then

$$M_x = M_a - (L\cos\alpha + D\sin\alpha)(a - x) \quad 2.63$$

Converting to coefficient form by dividing by $\frac{1}{2}\rho V^2 A$ gives

$$C_{MX} = C_{Ma} - (C_L\cos\alpha + C_D\sin\alpha)\left(\frac{a}{c} - \frac{x}{c}\right) \quad 2.64$$

With this equation it is easy to calculate C_{MX} , for any value of x/c . As a particular case, if the known pitching moment coefficient is that about the leading edge, C_{MLE} , then $a = 0$, and Eqn.2.64 becomes

$$C_{MX} = C_{MLE} + \frac{x}{c}(C_L\cos\alpha + C_D\sin\alpha) \quad 2.66$$

2.8.1 Aerodynamic centre

If the pitching moment coefficient at each point along the chord is calculated for each of several values of C_L , one very special point is found for which C_M is virtually constant, independent of the lift coefficient. This point is the aerodynamic centre. For incidences up to 10 degrees or so it is a fixed point close to, but not in general on, the chord line, between 23% and 25% of the chord behind the leading edge.

For a flat or curved plate in inviscid, incompressible flow the aerodynamic centre is theoretically exactly one quarter of the chord behind the leading edge; but thicknesses of the section, and viscosity of the fluid, tend to place it a few per cent further forward as indicated above, while compressibility tends to move it backwards. For a thin aerofoil of infinite aspect ratio in supersonic flow the aerodynamic centre is theoretically at 50% chord.

Knowledge of how the pitching moment coefficient about a point distance a behind the leading edge varies with C_L may be used to find the position of the aerodynamic centre behind the leading edge, and also the value of the pitching moment coefficient there, C_{MAC} let the position of the aerodynamic centre be a distance X_{ac} behind the leading edge. Then, with Eqn. 2.64 slightly rearranged,

$$C_{Ma} = C_{MAC} - (C_L \cos \alpha + C_D \sin \alpha) \left(\frac{X_{AC}}{c} - \frac{a}{c} \right) \quad 2.67$$

Now at moderate incidences, between say 3° and 7° :

$$C_L = O[20C_D] \quad \text{and} \quad \cos \alpha = O[10 \sin \alpha]$$

Where the symbol $O[]$ means of the order of, i.e. C_L is of the order of 20 times C_D .

Then

$$C_L \cos \alpha = O[200C_D \sin \alpha]$$

and therefore $C_D \sin \alpha$ can be neglected compared with $C_L \cos \alpha$. With this approximation and the further approximation $\cos \alpha = 1$,

$$C_{Ma} = C_{MAC} - C_L \left(\frac{X_{AC}}{c} - \frac{a}{c} \right) \quad 2.68$$

Differentiating Eqn. 2.68 with respect to C_L gives

$$\frac{d}{dC_L}(C_{Ma}) = \frac{d}{dC_L}(C_{MAC}) - \left(\frac{x_{AC}}{c} - \frac{a}{c}\right) \quad 2.69$$

But the aerodynamic centre is, by definition, that point about which C_M is independent of C_L , and therefore the first term on the right-hand side is identically zero, so that

$$\frac{d}{dC_L}(C_{Ma}) = 0 - \left(\frac{x_{AC}}{c} - \frac{a}{c}\right) = \frac{a}{c} - \frac{x_{AC}}{c} \quad 2.70$$

$$\frac{x_{AC}}{c} = \frac{a}{c} - \frac{d}{dC_L}(C_{Ma}) \quad 2.71$$

If, then, C_{Ma} is plotted against C_L , and the slope of the resulting line is measured, subtracting this value from a/c gives the aerodynamic centre position x_{ac}/c . In addition if, in Eqn. 2.64, C_L is made zero, that equation becomes

$$C_{Ma} = C_{MAC} \quad 2.72$$

i.e. the pitching moment coefficient about an axis at zero lift is equal to the constant pitching moment coefficient about the aerodynamic centre. Because of this association with zero lift, C_{MAC} is often denoted by C_{M0} . [1]

2.8.2 Centre of Pressure

The aerodynamic forces on an aerofoil section may be represented by a lift, a drag, and a pitching moment. At each value of the lift coefficient there will be found to be one particular point about which the pitching moment coefficient is zero, and the aerodynamic effects on the aerofoil section may be represented by the lift and the drag alone acting at that point. This special point is termed the centre of pressure.

Whereas the aerodynamic centre is a fixed point that always lies within the profile of a normal aerofoil section, the centre of pressure moves with change of lift coefficient and is not necessarily within the aerofoil profile. Figure 1.13 shows the forces on the aerofoil regarded as either

(a) lift, drag and moment acting at the aerodynamic centre; or

- (b) Lift and drag only acting at the centre of pressure, a fraction k_{CP} of the chord behind the leading edge.

Then, taking moments about the leading edge:

$$M_{LE} = M_{AC} - (L\cos\alpha + D\sin\alpha)X_{AC} = -(L\cos\alpha + D\sin\alpha)K_{CPC} \quad 2.73$$

Dividing this by $\frac{1}{2}\rho U_{\infty}^2 A$, it becomes

$$M_{AC} - (C_L\cos\alpha + C_D\sin\alpha)\frac{X_{AC}}{C} = -(C_L\cos\alpha + C_D\sin\alpha)K_{CPC} \quad 2.74$$

$$K_{CP} = \frac{X_{AC}}{C} = \frac{M_{AC}}{C_L\cos\alpha + C_D\sin\alpha} \quad 2.75$$

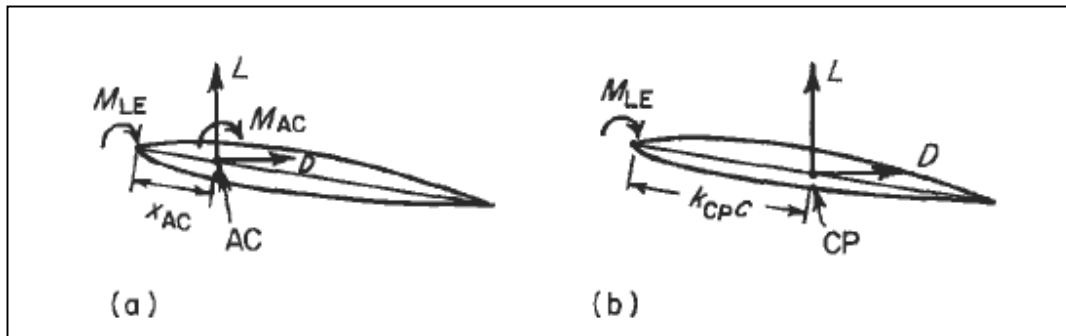


Figure 2.13 Forces on the aerofoil [1]

2.8 Profile theory for Very Thin Profiles (Skeleton Theory)

Fundamentals of skeleton theory the very thin profile (skeleton profile) is obtained by superposition of a translational flow with that of a distribution of plane potential vortices. This theory has therefore been termed the theory of the lifting vortex sheet. It was first developed by Birnbaum and Ackermann [15] and by Glauert [16], and later expanded in several treatises, particularly by Helmbold and Keune [17, 18], Allen [19], and Riegels [20].

For the following discussion a coordinate system as shown in Figure 2-14a is used. Accordingly, the profile chord coincides with the x axis. The coordinate system origin lies on the profile leading edge. The mean camber line is given by From Figure 2-14a, the mean camber line is seen to be covered with a continuous vortex distribution. With the assumption that the skeleton profile has only a slight camber and, therefore, rises only a little above the profile chord (x axis), the vortex distribution can be arranged on the chord instead of the mean camber line (Fig. 2.14b). The mathematical treatment of the problem is considerably simplified in this way.

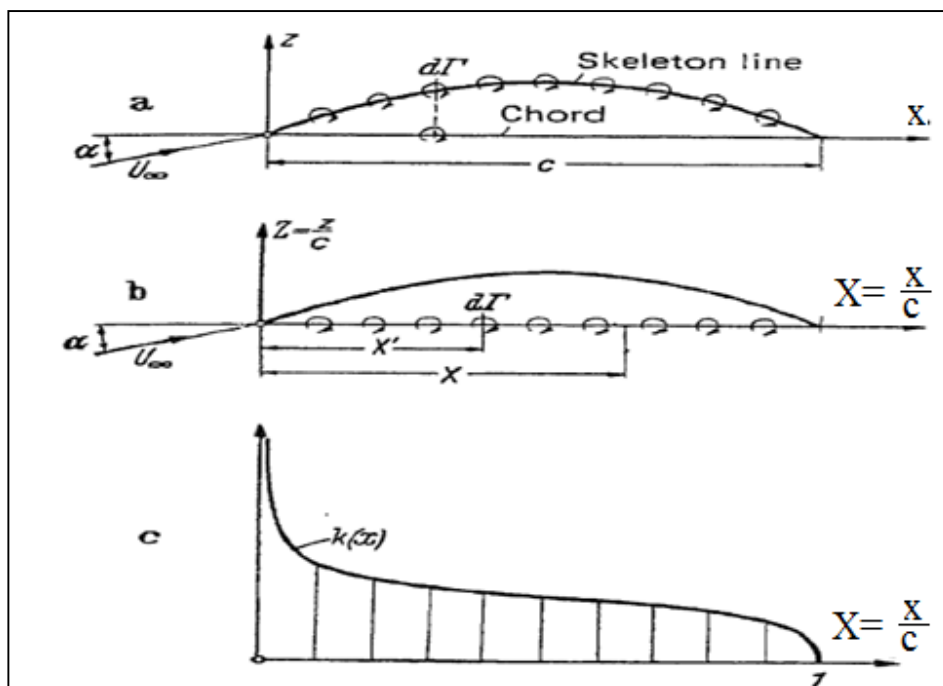


Figure 2-14 The skeleton theory. (a) Arrangement of the vortex distribution on the skeleton line. (b) Arrangement of the vortex distribution on the chord (slightly cambered profile), (c) Circulation distribution along the chord (schematic). [6]

The vortex strength of a strip of width dx of the vortex sheet is, from figure 2-14 b,

$$d\Gamma = k(x)dx \quad 2.77$$

Here, k is the vortex density (vortex strength per unit length) or the circulation distribution. By applying the law of Biot-Savart, the velocity components in the x and z directions, respectively, that are induced by the vortex distribution at station x , z are

$$u(x, z) = \frac{1}{2\pi} \int_0^c k(x') \frac{z}{(x - x')^2 + z^2} dx' \quad 2.78$$

$$w(x, z) = -\frac{1}{2\pi} \int_0^c k(x') \frac{x - x'}{(x - x')^2 + z^2} dx' \quad 2.79$$

Where

x' : Location of vortex strength at any point on chord

For slightly cambered profiles, the velocity components on the skeleton line are approximately equal to the values on the profile chord ($z = 0$). The velocity components on the chord are obtained through limit operations as $z \rightarrow 0$ of Eqs. 2.78 and 2.79

$$u(X) = \pm \frac{1}{2} k(X) \quad 2.80$$

$$w(X) = -\frac{1}{2\pi} \int_0^1 k(X') \frac{dX'}{X - X'} \quad 2.81$$

The dimensionless quantities

$$X = \frac{x}{c} \quad \text{and} \quad X' = \frac{x'}{c} \quad 2.82$$

The velocity component u is proportional to the vortex density. The upper sign is valid for the profile upper surface, the lower sign for the lower surface. When crossing the vortex sheet, the velocity component u changes abruptly by an amount

$$\Delta u = u_u - u_l = k \quad 2.83$$

The distribution of the vortex density on the chord is determined by the kinematic flow condition, which requires that the skeleton line is a streamline. Specifically, a translational velocity U_∞ is superimposed on the vortex distribution that forms the angle of attack with the chord (Figure 2-14).

The kinematic flow condition can also be formulated by the requirement that the velocity components normal to the mean camber line must disappear. Within the framework of the above approximation, it is sufficient to satisfy this condition on the chord instead of the mean camber line, resulting in

$$U_\infty \left[\alpha - \frac{dZ^s(X)}{dX} \right] + w(X) = 0 \quad 2.84$$

Where $Z^s = \frac{z^s}{c}$.

This equation relates the angle of attack α and the ordinates of the camber Z^s to the induced normal velocities w . The velocity distribution on the profile surface and the vortex density are related by

$$U(X) = U_\infty + u(X) = U_\infty \pm \frac{1}{2} k(X) \quad 2.85$$

This relationship is valid for small angles of attack according to Eq. 2.81.

The Kutta condition,

$$k=0 \text{ for } X=1 \quad 2.86$$

The total circulation around the profile is determined from the distribution of the vortex density as

$$\Gamma = \int_0^c k(x) dx = \int_0^1 k(X) dX \quad 2.87$$

The pressure difference between the lower and upper surface is obtained by means of the Bernoulli equation:

$$P_U - P_l = \rho U_\infty \Delta u = \rho U_\infty k \quad 2.88$$

With Eq. 2.48 the dimensionless pressure coefficient takes the form

$$\Delta C_p(X) = \frac{P_U - P_l}{q_\infty} = 2 \frac{k(X)}{U_\infty} \quad 2.89$$

With

$$q_\infty = \frac{\rho U_\infty^2}{2} \quad 2.90$$

Where

q_∞ : Dynamic pressure of undisturbed flow

being the dynamic pressure of the incident flow. Consequently, the distribution of the vortex density produces directly the load distribution over the profile chord, and the lift and moment coefficient are defined as follows:

$$C_L = \int_0^1 \Delta C_p(X) dX = \frac{2}{U_\infty} \int_0^1 k(X) dX \quad 2.91$$

$$C_M = - \int_0^1 \Delta C_p(X) X dX = - \frac{2}{U_\infty} \int_0^1 k(X) X dX \quad 2.92$$

2.9 Computation of the mean camber line from the distribution of circulation

Computation of the mean camber line from the distribution of circulation determining the shape of the mean camber line and the angle of attack from a given distribution of circulation $k(X)$ requires two steps. First, from

$$w(X) = - \frac{1}{2\pi} \int_0^1 k(X') \frac{dX'}{X - X'} \quad 2.93$$

Where $X' = \frac{x'}{c}$, the distribution of the induced downwash velocity $w(X)$ is obtained along the profile chord. Then, this distribution is introduced into the kinematic flow condition,

$$U_{\infty} \left[\alpha - \frac{dZ^S(X)}{dX} \right] + w(X) = 0 \quad 2.94$$

And the following expression for the shape of the mean camber line is obtained by integration over X:

$$Z^S(X) = \alpha X + \int_0^X \frac{w(X')}{U_{\infty}} dX' + C \quad 2.95$$

These two steps may be combined into one equation by introducing Eq. 2.93 into Eq. 2.95 and integrating over X. The angle of attack and the integration constant C is determined in such a way that the ordinates of the mean camber line disappear on the leading and trailing edges, resulting in

$$Z^S(X) = \alpha X - \frac{1}{2\pi} \int_0^1 \frac{K(X')}{U_{\infty}} \ln \left| \frac{X - X'}{X'} \right| dX' \quad 2.96$$

for the mean camber line and

$$\alpha = \frac{1}{2\pi} \int_0^1 \frac{K(X')}{U_{\infty}} \ln \left| \frac{X - X'}{X'} \right| dX' \quad 2.98$$

for the angle of attack as measured from the chord.

In the case of a constant distribution of circulation along the profile chord, $K = 2U_{\infty}C$, Eqs. 2.96 and 2.97 yield, for the mean camber line and the angle of attack,

$$Z^S(X) = -\frac{C}{\pi} [(1 - X) \ln(1 - X) + X \ln X] \quad \text{with } \alpha = 0 \quad 2.99$$

Where

C: is constant obtained by the integration of mean camber line

The maximum camber height is

$$h/c = (\ln 2/\pi) = 0.221 C \text{ and lies at 50\% chord} \quad 2.100$$

Following up on the investigations of Birnbaum and Ackermann, Glauert [18] proposed the following Fourier series expansion for the circulation distribution in the two-dimensional airfoil problem:

$$k(\varphi) = 2U_\infty \left(A_0 \tan \frac{\varphi}{2} + \sum_{n=1}^N A_n \sin n\varphi \right) \quad 2.101$$

$$X = \frac{1}{2}(1 + \cos\varphi) \quad 2.102$$

Where

φ : is the angle from the trailing edge to the location of the velocity distribution on upper or lower surface of airfoil

A_0, A_n : are Fourier series coefficient

So that on the leading edge $X=0$ and $\varphi=\pi$, and on the trailing edge $X=1$ and $\varphi=0$. Each term in Eq.2.101 satisfies the Kutta condition.

By introducing the expression for distribution of the circulation Eq.2.101 into equation for the induced downwash velocity Eq. 2.93 the simple relationship

$$\frac{w(\varphi)}{U_\infty} = - \left(A_0 + \sum_{n=1}^N A_n \cos n\varphi \right) \quad 2.103$$

is found after the integration. The interrelation of the Fourier coefficient of Eq.2.103, the shape of the mean line, and the angle of attack are obtained with the help of Eq. 2.94 as

$$A_0 + \sum_{n=1}^N A_n \cos n\varphi = \alpha - \frac{dZ^s(X)}{dX} \quad 2.104$$

With a given distribution of the circulation, this is a differential equation for the mean camber line $Z^s(X)$.

The first two terms in Eq. 2.101 represent particularly simple mean camber lines: The distribution of circulation of the first standard distribution becomes

$$k = k_1 A_0 = 2U_\infty A_0 \tan \frac{\phi}{2} = 2U_\infty A_0 \sqrt{\frac{1-X}{X}} \quad 2.105$$

Where k_1 is first standard distribution of the circulation. The distribution k is shown in Figure 2-15 a. The induced downwash velocity is determined from Eq. 2.83 to be $w/U_\infty = -A_0$, leading to

$$\frac{w_1}{U_\infty} = -1 \quad 2.106$$

Further, from the kinematic flow condition, Eq. 2-100, it follows that the profile inclination dZ^s/dX must be constant. This is possible only when $Z^s = 0$, and, therefore,

$$A_0 = \alpha \quad 2.107$$

It has thus been shown that the first normal distribution represents flow about the inclined flat plate. The second normal distribution is given by

$$k = k_{11} A_1 = 2U_\infty A_1 \sin \phi = 4U_\infty A_1 \sqrt{X(1-X)} \quad 2.108$$

Where k_{11} is the first normal distribution of the circulation and A_1 is Fourier series coefficient.

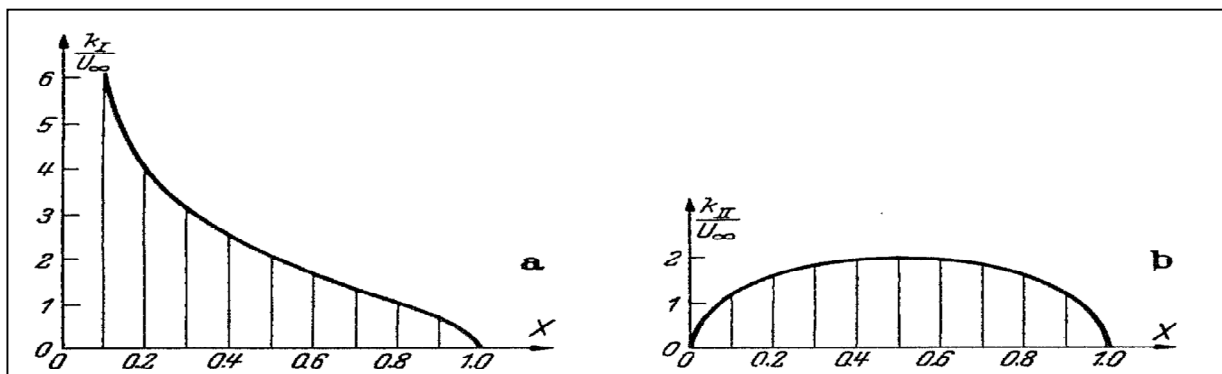


Figure 2.15 The first and the second normal distributions; circulation distribution by Eq. 2.101 (a) the inclined flat plate. (b) The parabolic skeleton at zero angle of incidence. [6]

This is an elliptic distribution (Fig. 2.15b). The induced downwash velocity is obtained from Eq. 2.103 as

$$\frac{w_{11}}{U_{\infty}} = -\cos\varphi = -(2X - 1) \quad 2.109$$

Where w_{11} is the downwash velocity for the elliptic distribution, and with Eq. 2.95, the shape of the mean camber line is given by

$$Z^s = A_1 X(1 - X) = 4 \frac{h}{c} X(1 - X) \quad \text{with } \alpha = 0 \quad 2.110$$

This is a parabolic mean camber line with camber height $h/c = A_1/A_0$.

2.10 Computation of the aerodynamic coefficients

Computation of the aerodynamic coefficients equations will now be presented that allow one to compute the aerodynamic coefficients directly from a given mean camber line. The lift coefficient is obtained from Eq. 2.91 after integration with the help of Eqs. 2.101 and 2.102 for the distribution of circulation as

$$C_L = \pi(2A_0 + A_1) \quad 2.111$$

In the same way, the pitching-moment coefficient relative to the leading edge is obtained from Eq.2.92 as

$$C_M = -\frac{\pi}{4}(2A_0 + 2A_1 + A_2) \quad 2.112$$

Where A_0, A_1, A_2 is Fourier series coefficient. This equation was first presented by Munk [21].

The angle of attack for zero lift ($C_L = 0$) is obtained by setting $2A_0 = -A_1$ and the zero-lift moment coefficient becomes $c_{M0} = -(\pi/4)(A_1 + A_2)$. Consequently, the pitching-moment coefficient can also be written as

$$C_M = C_{M0} - \frac{1}{4}C_L \quad 2.113$$

From Eq. (1-29), the neutral-point location is given by $-dc_M/dc_L = x_N/c$. Consequently, the distance of the neutral point from the leading edge becomes

$$\frac{x_N}{c} = \frac{1}{4} \quad 2.114$$

Which is independent of the shape of the mean camber line. The Fourier coefficients are found through Fourier analysis:

$$A_0 = \alpha - \frac{1}{\pi} \int_0^\pi \frac{dZ^s}{dX} d\varphi \quad A_1 = \alpha - \frac{2}{\pi} \int_0^\pi \frac{dZ^s}{dX} \cos n\varphi d\varphi \quad (n \geq 1) \quad 2.115$$

The integrals can be transformed through integration by parts into terms in which the camber line coordinates Z^s replace the camber line inclination dZ^s/dX . By introducing the coefficients A_0 and A_1 into Eq. 2.113 the relation

$$\frac{dC_L}{d\alpha} = 2\pi \quad 2.116$$

is obtained for the lift slope, independent of the camber line shape, and the lift coefficient

$$C_L = \frac{dC_L}{d\alpha} (\alpha - \alpha_0) = 2\pi(\alpha - \alpha_0) \quad 2.117$$

The equations for α_0 , lift coefficient and zero moment are given in Table 2-2.

Table 2-2 Compilation of formulas for the aerodynamic coefficients of cambered profiles of finite thickness. [6]

Lift slope	$\frac{dC_L}{d\alpha}$	$2\pi \left(1 + \frac{2}{\pi} \int_0^\pi \frac{Z^t}{\sin\phi} d\phi \right)$	$2\pi \left(1 + 2 \sum_1^{N-1} A_m Z_m^t \right)$
Zero-lift angle	α_0	$\frac{-2}{\pi} \int_0^\pi \frac{Z^s}{1 - \cos\phi} d\phi$	$2 \sum_1^{N-1} B_m Z_m^s$
Neutral-point location	$\frac{X_N}{c}$	$\frac{1}{4} \left(1 + \frac{2}{\pi} \int_0^\pi \frac{1 + 2\cos\phi - 2\cos 2\phi}{\sin\phi} Z^t d\phi \right)$	$\frac{1}{4} \left(1 + 2 \sum_1^{N-1} C_m Z_m^t \right)$
Zero moment	C_{M0}	$-\int_0^\pi \frac{2\cos\phi - \cos 2\phi}{1 - \cos\phi} Z^s d\phi$	$2 \sum_1^{N-1} D_m Z_m^s$

In the integral formulas of Table 2-2 for the computation of the various coefficients, only the distribution of the mean camber coordinates $Z^s(\phi)$ appear besides certain trigonometric functions (also called circular functions are functions of an angle. They are used to relate the angles of a triangle to the lengths of the sides of a triangle. Trigonometric) of ϕ . In addition, simple quadrature formulas are given for the numerical evaluation of the integrals. Accordingly, the profile coordinates $Z_m = Z(X_m)$, at the stations X_m are multiplied with once-for-all-computed coefficients A_m, \dots, F_m , and the sums are then formed of these products (see Table 2-3). [6]

Where Z_m is dimensionless and Z coordinates of the upper or lower of airfoil surface at location X_m .

Table 2-3 Coefficient A, B, C, D, E, F for the computation of the aerodynamic coefficient of table 2-2 for N=12 (after Riegels [22, 23]) [6]

m	X_m	A_m	B_m	C_m	D_m	E_m	F_m
1	0.9830	0.6440	-4.8919	0.6864	-7.9370	-2.4032	15.6333
2	0.9330	0	0	0.1667	-0.2267	0	0
3	0.8536	0.2357	-0.5690	0.3333	-1.0790	-0.2357	2.0944
4	0.7500	0	0	0.2887	-0.1309	0	0
5	0.6294	0.1726	-0.2249	0.2387	-0.4210	-0.0462	1.1224
6	0.5000	0	0	0.3333	0	0	0
7	0.3706	0.1726	-0.1324	0.0601	-0.1402	0.0462	1.1224
8	0.2500	0	0	0.2887	0.1309	0	0
9	0.1465	0.2357	-0.0976	0.3333	0.0318	0.2357	2.0944
10	0.0670	0	0	0.1667	0.2267	0	0
11	0.0170	0.6439	-0.0848	-1.8017	0.1197	2.4032	15.6333

2.11 Velocity distribution and Pressure distribution

2.11.1 Computation the velocity distribution on the skeleton line

The problem of computing the distribution of the circulation and consequently the velocity distribution will now be treated for a given skeleton line shape at a given angle attack. By introducing

$$U_\infty \left[\alpha - \frac{dZ^S(X)}{dX} \right] + w(X) = 0 \quad 2.122$$

Into

$$w(X) = -\frac{1}{2\pi} \int_0^1 k(X') \frac{dX'}{X - X'} \quad 2.123$$

The equation defining the circulation distribution becomes

$$U_\infty \left[\alpha - \frac{dZ^S(X)}{dX} \right] = \frac{1}{2\pi} \int_0^1 k(X') \frac{dX'}{X - X'} \quad 2.124$$

This is an integral equation for the vortex density K with given values of $\alpha - dZ^S(X)/dX$. It was first solve by Betz. By taking into account the Kutta condition:

$$k = 0 \quad \text{for } X = 0 \quad 2.125$$

And

$$U(X) = U_\infty + u(X) = U_\infty \pm \frac{1}{2}k(X) \quad 2.126$$

The velocity distribution about the skeleton profile is given by

$$\frac{U(X)}{U_\infty} = 1 \pm \sqrt{\frac{1-X}{X}} \left(\alpha + \frac{1}{\pi} \int_0^1 \frac{dZ^S}{dX'} \sqrt{\frac{1-X'}{X'}} \frac{dX'}{X-X'} \right) \quad 2.127$$

To evaluate the quadrature formula for the velocity distribution, Riegels makes the Fourier substitution

$$Z^S = \frac{1}{2} \sum_{v=1}^n a_v \cos v\varphi \quad 2.128$$

$$X = \frac{1}{2} (1 + \cos\varphi) \quad 2.129$$

Where a_v is Fourier series coefficient. Introducing these expressions into Eqs. 2.127 makes elementary evaluation of the integrals possible. The velocity distribution of the skeleton profile is then

$$\frac{U(\varphi)}{U_\infty} = 1 \pm \left(\alpha \tan \frac{\varphi}{2} + \sum_{v=1}^n v a_v \frac{\cos v\varphi - 1}{\sin\varphi} \right) \quad 2.130$$

Where the upper sign is valid for the upper side, the lower sign for lower side of the skeleton profile. [6]

Eqs. 2.127 give the velocity distribution for skeleton profile, but the whole velocity distribution over any profile is consisting of

1. Symmetrical profile without angle of attack.
2. Symmetrical profile with angle of attack.
3. Skeleton profile without angle of attack, and

4. Plate with angle of attack.

The derivation of the other three velocity distribution are not derived here, it derives on Aerodynamic of the Airplane book [6].

The velocity distribution over any profile given as

$$\frac{W_k(X)}{U_\infty} = \frac{1}{x(X)} \left[\underbrace{1 + \frac{1}{\pi} \int_0^1 \frac{dZ^t}{dX'} \frac{dX'}{X - X'}}_{\text{Symmetrical profile}} \pm \underbrace{\frac{1}{\pi} \sqrt{\frac{1-X}{X}} \int_0^1 \frac{dZ^s}{dX'} \sqrt{\frac{X'}{1-X'X-X'}}}_{\text{Skeleton profile}} \right. \\ \left. \pm \alpha \sqrt{\frac{1-X}{X}} \left(1 + \frac{1}{\pi} \int_0^1 \left(\frac{dZ^t}{dX'} - \frac{Z^t}{2X'(1-X')} \right) \frac{dX'}{X - X'} \right) \right]$$

Plate with angle of attack

2.131

2.11.2 Pressure distribution for given lift coefficient and moment coefficient

Pressure distribution for given lift coefficient and moment coefficient the problem of approximating a given skeleton line by superposition of an inclined flat plate and a parabolic skeleton in such a way that lift and zero-moment coefficients of approximation and given skeleton are equal can be solved with the help of the above-introduced Fourier series expansion. In this case the Fourier coefficients from Eqs. 2.95 and 2.96 become

$$A_0 = \frac{1}{2\pi} C_L + \frac{2}{\pi} C_{M0} \quad \text{and} \quad A_1 = -\frac{4}{\pi} C_{M0}$$

2.132

Where A_0, A_1 are Fourier series coefficients, and by using table 2.2 to calculate lift coefficient (C_L) and zero moment (C_{M0}). These coefficients are introduced into Eq. 2.101 and the resultant pressure distribution, taking into account Eq. 2.2.89 is obtained as

$$\Delta C_p(X) = C_L h_0(X) + C_{M0} 4h_1(X)$$

2.133

With

$$h_0(X) = \frac{2}{\pi} \sqrt{\frac{1-X}{X}} \quad \text{and} \quad h_1(X) = \frac{2}{\pi} (1-4X) \sqrt{\frac{1-X}{X}} \quad 2.134$$

Where h_0, h_1 are Fourier series coefficients. The distributions $h_0(X)$ and $h_1(X)$ are shown in Figure 2.16

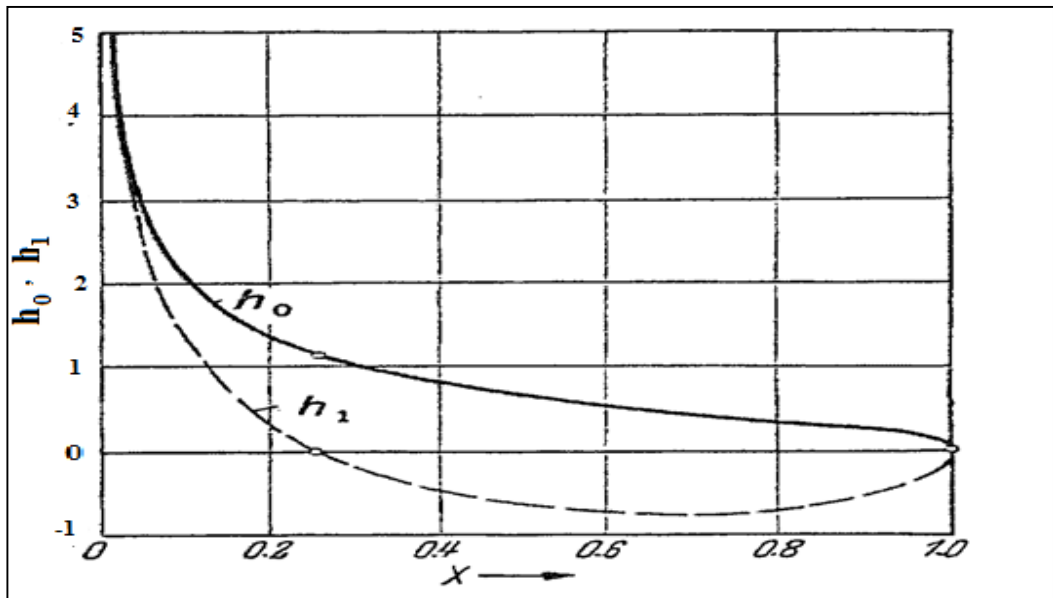


Figure 2.16 The function h_0 and h_1 for pressure distribution on the chord at given lift and moment coefficient [Eqs.2.111 and 2.112]. [6]

CHAPTER 3

NUMERICAL ANALYSIS OF PROFIL THEORY

In the previous chapters the solution to the parameter of the airfoils was obtained by analytical techniques. The application of numerical techniques allows the treatment of more realistic geometries. In this chapter the methodology of some numerical solutions will be examined and applied to calculate the parameter of the airfoils.

3.1 Estimation coefficient lift and drag from pressure coefficient

Let Figure 3.1 represent an aerofoil at an angle of incidence α to a fluid flow travelling from left to right at speed V . The axes O_x and O_z are respectively aligned along and perpendicular to the chord line. The chord length is denoted by c .

Taking the aerofoil to be a wing section of constant chord and unit spanwise length, let us consider the forces acting on a small element of the upper aerofoil surface having length δs . The inward force perpendicular to the surface is given by $P_u \delta s$. This force may be resolved into components δX and δZ in the x and z directions. It can be seen that

$$\delta Z_u = -P_u \cos \epsilon \quad 3.1$$

and from the geometry

$$\delta s \cos \epsilon = \delta x \quad 3.2$$

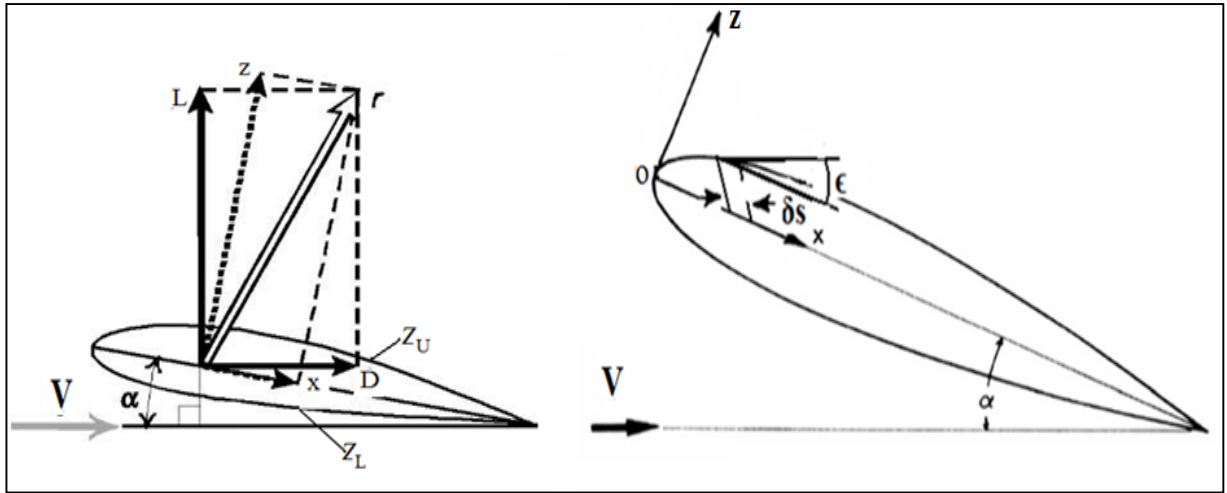


Figure 3.1 Normal pressure force on an element of aerofoil surface [24]

so that

$$\delta Z_u = -P_u \delta x \quad \text{per unit span} \quad 3.3$$

Similarly, for the lower surface

$$\delta Z_l = -P_l \delta x \quad \text{per unit span} \quad 3.4$$

We now add these two contributions and integrate with respect to x between $x = 0$ and $x = c$ to get

$$Z = - \int_0^c P_u dx + \int_0^c P_l dx \quad 3.5$$

But we can always subtract a constant pressure from both P_u and P_l without altering the value of Z , so we can write

$$Z = - \int_0^c (P_u - P_\infty) dx + \int_0^c (P_l - P_\infty) dx \quad 3.6$$

Where P_∞ is the pressure in the free stream (we could equally well use any other constant pressure, e.g. the stagnation pressure in the free stream).

Equation 3.6 can readily be converted into coefficient form. Recalling that the aerofoil section is of unit span, the area $A = 1 \times c = c$ so we obtain

$$\begin{aligned}
C_Z &= \frac{Z}{\frac{1}{2}\rho U_\infty^2 c} = \frac{1}{\frac{1}{2}\rho U_\infty^2 c} \left[-\int_0^c (P_u - P_\infty) dx + \int_0^c (P_l - P_\infty) dx \right] \\
&= \frac{-1}{\frac{1}{2}\rho U_\infty^2 c} \int_0^c [(P_u - P_\infty) - (P_l - P_\infty)] dx
\end{aligned} \tag{3.7}$$

Remembering that $(1/c)dx = d(x/c)$ and that the definition of pressure coefficient is

$$C_p = \frac{P - P_\infty}{\frac{1}{2}\rho U_\infty^2 c} \tag{3.8}$$

We see that

$$C_Z = -\int_0^1 (P_u - P_l) d\left(\frac{x}{c}\right) \tag{3.9}$$

Similar arguments lead to the following relations for X.

$$\delta X_u = P_u \delta s \sin \epsilon \quad \delta X_l = P_l \delta s \sin \epsilon \quad \delta s \sin \epsilon = \delta z$$

Giving

$$C_X = \oint_c C_p d\left(\frac{z}{c}\right) = \int_{Z_{ml}}^{Z_{mu}} \Delta C_p d\left(\frac{z}{c}\right) \tag{3.10}$$

Where Z_{mu} and Z_{ml} are respectively the maximum and minimum values of z , and ΔC_p , is the difference between the values of C_p acting on the fore and rear points of an aerofoil for a fixed value of z . [11]

C_Z and C_X are the force coefficients in the Z and X directions, C_{pl} and C_{pu} are the pressure coefficients on the lower and upper surface, and C_{pf} and C_{pa} are the pressure coefficients forward and aft of the point of maximum thickness on the airfoil. The force coefficients were found by numerically integrating using the trapezoidal rule.

$$C_Z = \left[\sum_{i=1}^{\infty} \left(\frac{C_{pi} + C_{pi+1}}{2} \right) \left| \frac{x_i}{c} - \frac{x_{i+1}}{c} \right| \right]_{\text{upper}} - \left[\sum_{i=1}^{\infty} \left(\frac{C_{pi} + C_{pi+1}}{2} \right) \left| \frac{x_i}{c} - \frac{x_{i+1}}{c} \right| \right]_{\text{lower}} \tag{3.11}$$

$$C_X = \left[\sum_{i=1}^{\infty} \left(\frac{C_{pi} + C_{pi+1}}{2} \right) \left| \frac{x_i}{c} - \frac{x_{i+1}}{c} \right| \right]_{\text{FRONT}} - \left[\sum_{i=1}^{\infty} \left(\frac{C_{pi} + C_{pi+1}}{2} \right) \left| \frac{x_i}{c} - \frac{x_{i+1}}{c} \right| \right]_{\text{AFT}} \tag{3.12}$$

Once the force coefficients were calculated, the lift and drag coefficients were found by using Eq. 3.13 and Eq. 3.14.

$$C_L = C_Z \cos \alpha - C_X \sin \alpha \quad 3.13$$

$$C_D = C_Z \sin \alpha + C_X \cos \alpha \quad 3.14$$

C_L and C_D are the force coefficients in the lift and drag directions as seen in Figure 3.1. Furthermore, α is the angle of attack or the angle between the chord and the direction of airflow in the wind tunnel. All equations were obtained from Clancy [25] with the exception of Eq. 3.11 and 3.12 which were obtained from Aerodynamic Forces on Airfoils [26].

3.2 Numerical Evaluation of the Profile Theory

The calculations of the velocity distribution and the aerodynamic coefficient have been derived through the singularity method in the previous chapters. Now, these parameters can be evaluated in a convenient way through the numerical summation formulas. The details of the calculation are referred to the work of F.Riegels and E. Truckenbrodt. [6]

For the numerical quadrature the coordinates of the profile at the N-discrete nodes is determined as;

$$X_m = \frac{1}{2} \left(1 + \cos \frac{\pi m}{N} \right), \quad m = 0, 1, \dots, N \quad 3.15$$

And denoted with $Z(X_m) = Z_m$.

If $m=0$, it means the profile at trail edge whereas if $m=N$, it means the profile front, see table 3.1. In the table 3.1 n and m are running from 0 to 12, where the node 0 ($\varphi=0^\circ$) means the first node at profile trailing edge, and the node 12 ($\varphi=180^\circ$) is lying at the front leading edge of the profile. X_n and X_m are denoted the locations of the nodes, a_n , b_n , and c_n are served to calculate the velocity distribution of the profile.

The velocity distribution on the profile contour at discrete points X_n is obtained through the following summation formula;

$$\frac{W_k(X_n)}{U_\infty} = \frac{1}{X_n^*} \left[a_n + 2 \sum_{m=1}^{N-1} A_{nm} Z_m^t \pm 2 \sum_{m=1}^{N-1} C_{nm} Z_m^s \pm \alpha \left(b_n + 2 \sum_{m=1}^{N-1} H_{nm} Z_m^t \right) \right] \quad 3.16$$

Where

$$X_n^* = \sqrt{C_n + \left(\frac{dZ^t}{d\phi}\right)_n^2} \quad 3.17$$

Coefficient a_n, b_n, c_n which appear in the equation 3.16 and 3.17 are summarized in table 3.1. The coefficient with double subscripts A_{nm}, C_{nm} and H_{nm} which serve to determine the velocity distribution are given in table 3.2.

The aerodynamic parameters which are given in table 2.1 can also be calculated with the summation formulas.[26]

The in the summation formulas appearing coefficient are obtained from table 2.2.

Table 3.1 Coefficients a_n, b_n, c_n to calculate the velocity distribution on the contour profile according to Eq. 3.15 for $N = 12$ (after [27])

n,m	ϕ	X_n, X_m	a_n	b_n	c_n
0	0°	1.0000	0	0	0
1	15°	0.9830	0.1294	0.0170	0.0168
2	30°	0.9330	0.2500	0.0670	0.0625
3	45°	0.8536	0.3536	0.1464	0.1250
4	60°	0.7500	0.4330	0.2500	0.1875
5	75°	0.6294	0.4830	0.3706	0.2333
6	90°	0.5000	0.5000	0.5000	0.2500
7	105°	0.3706	0.4830	0.6294	0.2333
8	120°	0.2500	0.4330	0.7500	0.1875
9	135°	0.1465	0.3536	0.8536	0.1250
10	150°	0.0670	0.2500	0.9330	0.0625
11	165°	0.0170	0.1294	0.9830	0.0168
12	180°	0	0	1.0000	0

Table 3.2 Coefficients A_{nm} , C_{nm} , H_{nm} to calculate the velocity distribution on the profile contour of Eq. 3.15 for $N = 12$ (after [27])

	$\begin{matrix} n \\ m \end{matrix}$	1	2	3	4	5	6
A_{nm}	1	3	-1.0806	0	-0.086	0	-0.0231
	2	-1.0806	3	-1.1666	0	-0.1092	0
	3	0	-1.1666	3	-1.1897	0	-0.1179
	4	-0.086	0	-1.1897	3	-1.1984	0
	5	0	-0.1092	0	-1.1984	3	-1.2016
	6	-0.0231	0	-0.1179	0	-1.2016	3
	7	0	-0.0318	0	-0.1211	0	-1.2016
	8	-0.0087	0	-0.035	0	-0.1211	0
	9	0	-0.0119	0	-0.035	0	-0.1179
	10	-0.0032	0	-0.0119	0	-0.0318	0
	11	0	-0.0032	0	-0.0087	0	-0.0231
C_{nm}	1	5.4454	-1.3651	0.2845	-0.1985	0.1124	-0.0893
	2	1.0806	3	-0.9945	0	-0.0629	0
	3	2.4457	-1.279	3.2845	-1.2559	0.1124	-0.1667
	4	2.2475	0	-0.9714	3	-1.1348	0
	5	2.4457	-0.1754	0.2845	-1.2472	3.1124	-1.244
	6	2.3563	0	0.1179	0	-1.1316	3
	7	2.4457	-0.0806	0.2845	-0.1635	0.1124	-1.244
	8	2.3882	0	0.2071	0	-0.051	0
	9	2.4457	-0.0543	0.2845	-0.0774	0.1124	-0.1667
	10	2.4001	0	0.2302	0	0.0318	0
	11	2.4457	-0.0456	0.2845	-0.0575	0.1124	-0.0893
H_{nm}	1	0.7113	-0.3544	0.1003	-0.091	0.0538	-0.0469
	2	0.1422	0.8039	-0.4119	0	-0.0483	0
	3	0.3155	-0.3296	1.3403	-0.6969	0.0488	-0.1178
	4	0.2958	0	-0.4024	1.7321	-0.8708	0
	5	0.3133	-0.0293	0.0904	-0.682	2.3375	-1.1778
	6	0.3102	0	0.0488	0	-0.8683	3
	7	0.3072	0.0085	0.0713	-0.0295	0	-1.1316
	8	0.3144	0	0.0858	0	-0.0392	0
	9	0.2845	0.0617	0	0.1196	-0.132	0.1178
	10	0.316	0	0.0954	0	0.0244	0
	11	0	0.6431	-0.8952	1.3788	-1.7903	2.3563

	n		7	8	9	10	11
	m						
A_{nm}	1		0	-0.0087	0	-0.0032	0
	2		-0.0318	0	-0.0119	0	-0.0032
	3		0	-0.035	0	-0.0119	0
	4		-0.1211	0	-0.035	0	-0.0087
	5		0	-0.1211	0	-0.0318	0
	6		-1.2016	0	-0.1179	0	-0.0231
	7	3	-1.1984	0	-0.1092	0	0
	8	-1.1984	3	-1.1807	0	-0.086	0
	9	0	-1.1897	3	-1.1666	0	0
	10	-0.1092	0	-1.1666	3	-1.0806	0
	11	0	-0.086	0	-1.0806	3	0
C_{nm}	1		0.0662	-0.0575	0.0488	-0.0456	0.0424
	2		-0.0144	0	-0.0055	0	-0.0032
	3		0.0662	-0.0774	0.0488	-0.0543	0.0424
	4		-0.0973	0	-0.0286	0	-0.0151
	5		0.0662	-0.1635	0.0488	-0.0806	0.0424
	6		-1.1778	0	-0.1179	0	-0.0469
	7	3.0662	-1.2472	0.0488	-0.1754	0.0424	0
	8	-1.181	3	-1.2071	0	-0.1561	0
	9	0.0662	-1.2559	3.0488	-1.279	0.0424	0
	10	-0.1092	0	-1.2302	3	-1.3227	0
	11	0.0662	-0.1985	0.0488	-1.3651	3.0424	0
H_{nm}	1		0.0301	-0.0262	0.0155	-0.012	0
	2		-0.0188	0	-0.0132	0	-0.0244
	3		0.0227	-0.0495	0	-0.0204	-0.0488
	4		-0.1267	0	-0.069	0	-0.1148
	5		0	-0.1685	-0.042	-0.0539	-0.1808
	6		-1.535	0	-0.2845	0	-0.3565
	7	3.8495	-1.1966	-0.1535	-0.2349	-0.5319	0
	8	-1.5392	5.1962	-2.9142	0	-1.1865	0
	9	-0.2845	-1.6826	6.6737	-3.7117	-1.839	0
	10	-0.1423	0	-2.97	11.1962	10.0469	-
	11	-3.1009	3.8922	-5.7864	4.0326	4.5328	0

CHAPTER 4

RESULTS AND DISCUSSIONS

The design of an airfoil usually starts with the definition of the desired or required characteristics. The selection of an airfoil for a wind car depends mainly on the lift and drag characteristics of the airfoil. During this work, we can calculate;

- Velocity and pressure distribution
- Lift and drag coefficient
- Lift and drag forces and
- Total torque for various airfoil sections.

The purpose of this work is to study the aerodynamic characteristics. Several different airfoil profiles are available for study.

4.1 General Design Layout

Wind car is the kind of car power by natural wind energy. The main objective is to convert the wind energy to mechanical energy to overcome load that rotates the main shaft.

The basic task is conversion and storage of wind energy. There are many ways to convert and store wind energy to mechanical energy.

In this project, the three blade wind car is shown in figure 4. 1and the direct connection is used via various links and gear is shown in figure 4.1. A vertical wind turbine is mounted on the chassis. The turbine captures wind and moves due to the present of lift forces, which cause it to rotate about it fix axis.

As shown in figure 4.2 the axial rotation from the turbine is brought down by a vertical shaft hold and branched by a bearing. Double and single row deep groove ball bearings are selected because the feature higher load rating than single row bearings, but are very sensitive. The

rotation is then changed at 90° using a bevel gear. Figure 4.4 shown Bevel gears are gears where the axes of the two shafts intersect and the tooth-bearing faces of the gears themselves are conically shaped. Bevel gears are most often mounted on shafts that are 90 degrees apart, but can be designed to work at other angles as well. The pitch surface of bevel gears is a cone. It used to transmit motion between the shafts with intersection center lines. The intersection angle is normally 90° but may be as high as 180°. To control the direction of the car direct steering types see figure 4.3 is used. It makes use of the face gears which are a circular disc with a ring of teeth cut on one side. The gear teeth are tapered toward the center of the tooth. These gears typically mate with a spur gear. A special kind of scooter tires is used as our rotating wheels.

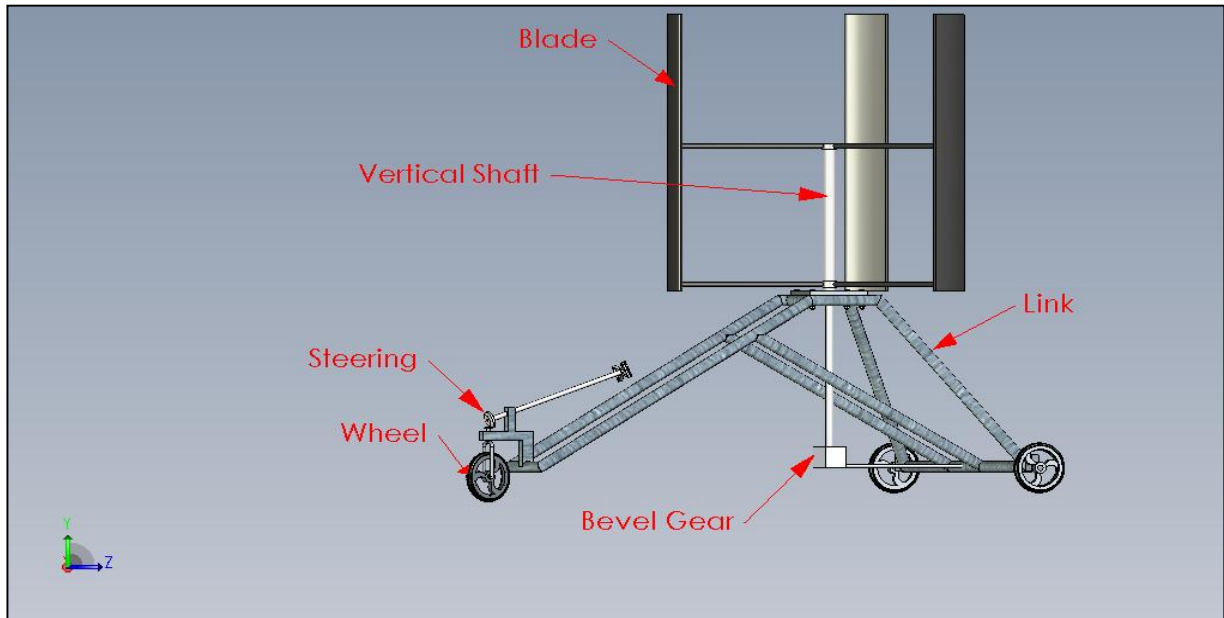


Figure 4.1 Three dimension of wind car

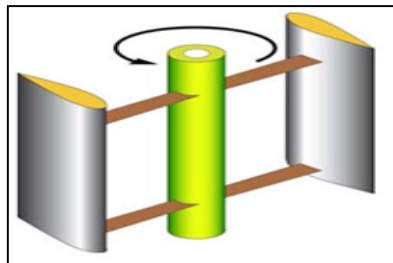


Figure 4.2 Rotaion of the blade

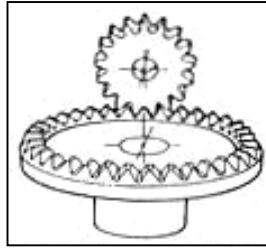


Figure 4.3 Steering

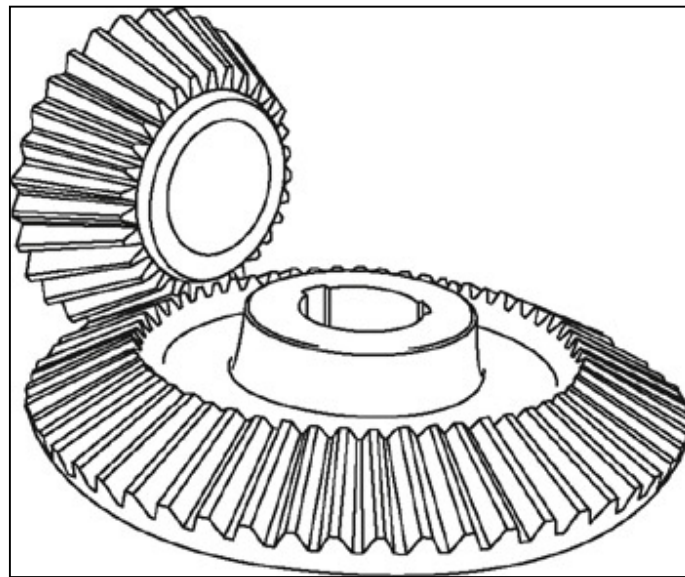


Figure 4.4 Bevel gear

4.2 Forces analysis during the rotation of the blades

For the following explanations, it is assumed, that a stream of air is directed against an airfoil, which is fixed in space. This is equivalent to an airfoil moving through the air just a question of the reference system. A typical wind tunnel works in the same way. The air was assumed to be incompressible. The viscous effects due to the surface of the airfoil at the test velocity were neglected because the surface of the airfoil was smooth.

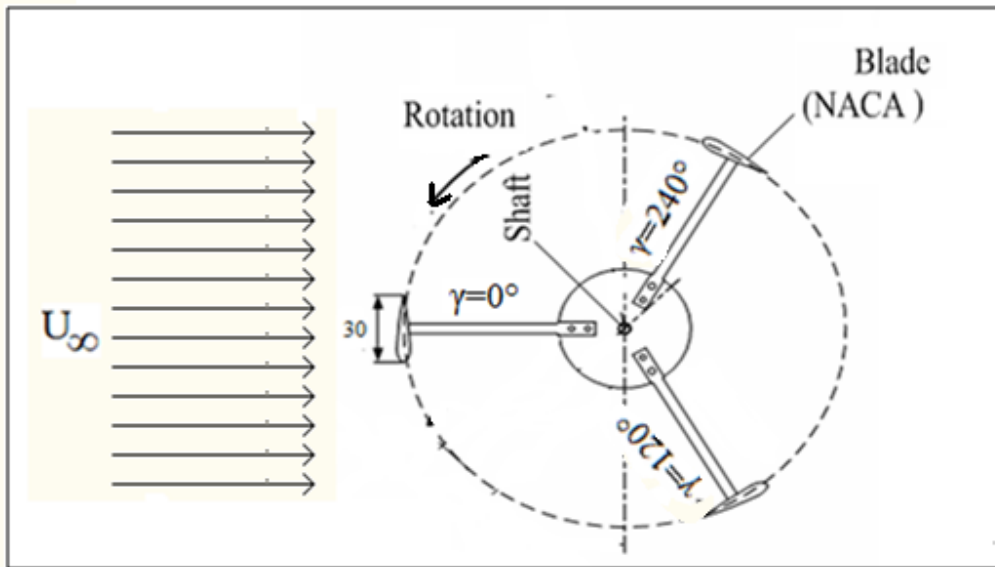


Figure 4.5 Schematic diagram of three-blade rotor

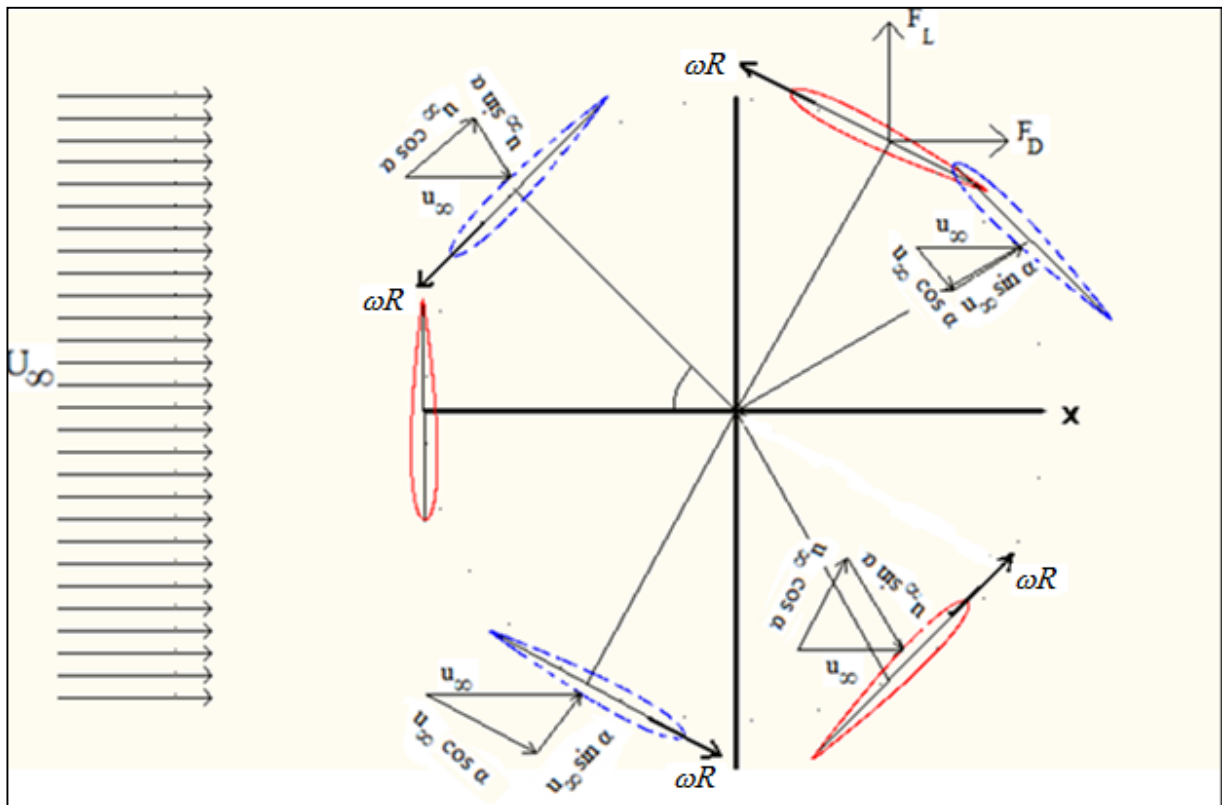


Figure 4.6 Forces analysis for the blades during the rotation

Figure 4.5 shows the free stream velocity U_∞ , the direction of speed of the blades (ωR), the position of the blades with angle γ , and the direction of rotation of the blades.

During the rotation, the free stream velocity has two components. The direction of the components changes as shown in figure 4.6. We can describe it as:

- First component, it is parallel to the chord line. We used it to calculate the skin friction drag force.
- Second component, it is perpendicular to the first one. We used it to calculate the pressure drag force.

Since the speed of the blades affects on both surfaces of the profile, and at the same time we have free stream velocity effect on the upper or lower surface which depends on the location of the profile. Sometimes, we subtract or add the free stream velocity to the speed of the blade, which depends on the direction of the velocity as shown in figure 4.7.

We can analysis the forces as follow:

1. From 0° to 90°

At 0° we have maximum pressure drag force on the upper surface of the profile. It can be calculated by using Eq. 2.51. In this case, the drag coefficient is equal to 2 (from table 2.1).

At 90° we have maximum skin friction drag in both surfaces of the profile. It can be calculated by using Eq. 2.51. In this case we replace C_D by C_f . The skin friction coefficient is 0.1 (from table 2.1).

2. From 90° to 180°

The free stream velocity has an effect on the lower surface of the profile. At 180° we have maximum pressure force on the lower surface.

3. From 180° to 270°

We can divide into two regions as:

- from 180° to 254°

In this region, the free stream velocity has an effect on the lower surface of the profile. And we have skin friction and pressure forces on the lower surface of the profile.

- from 254° to 270°

In this region, we have lift and drag forces. The lift and drag forces depend on the lift coefficient and drag coefficient respectively which depends on the angle of attack (α). Drag coefficient can be calculated using Eq. 2.53b and we took $C_{D,0}$ as 0.004 [28]. At 254° ($\alpha=16^\circ$) we have maximum lift and drag forces. At 270° lift force is equal to zero, but at the same time we have skin drag coefficient.

4. From 270° to 360°

In this case, the free stream velocity has an effect on the upper surface of the profile. At 360° we have maximum pressure force on the upper surface.

The same procedure is applied on the second and third blades. The blades are decaled by 120° between each other as shown in figure 4.5.

After analysis, the forces and the calculations of the forces for each location or position for the blade in both directions x and y axis are shown in figure 4.7. we can calculate the torque using equation 4.1.

$$\vec{T} = \sum \vec{F} \vec{r} \tag{4.1}$$

Where,

\vec{T} : is the torque vector and T is the magnitude of the torque, [N.m]

\vec{r} : is the displacement vector (a vector from the point from which torque is measured to the point where force is applied), [m]

F: is the force vector, and F is the magnitude of the force, [N]

For the reason of simplification, pressure forces through the rod are negligible.

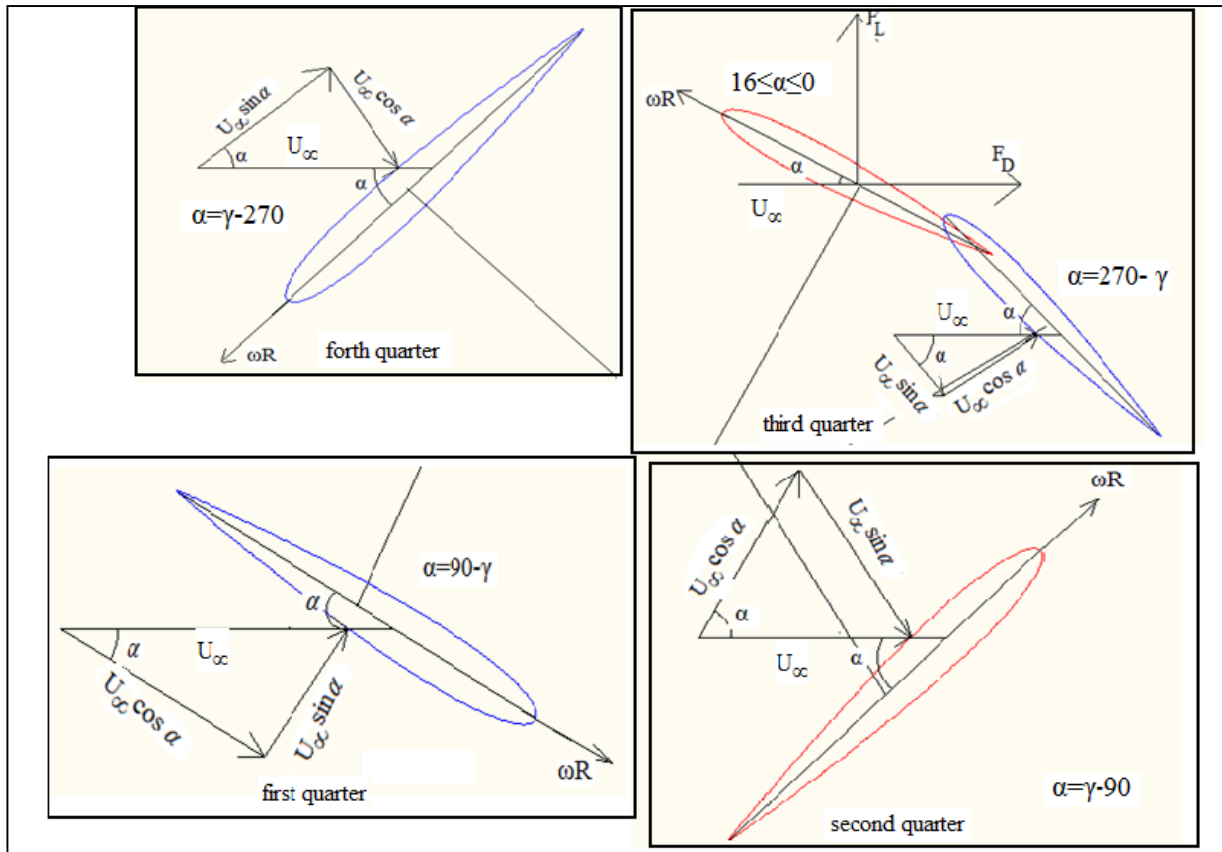
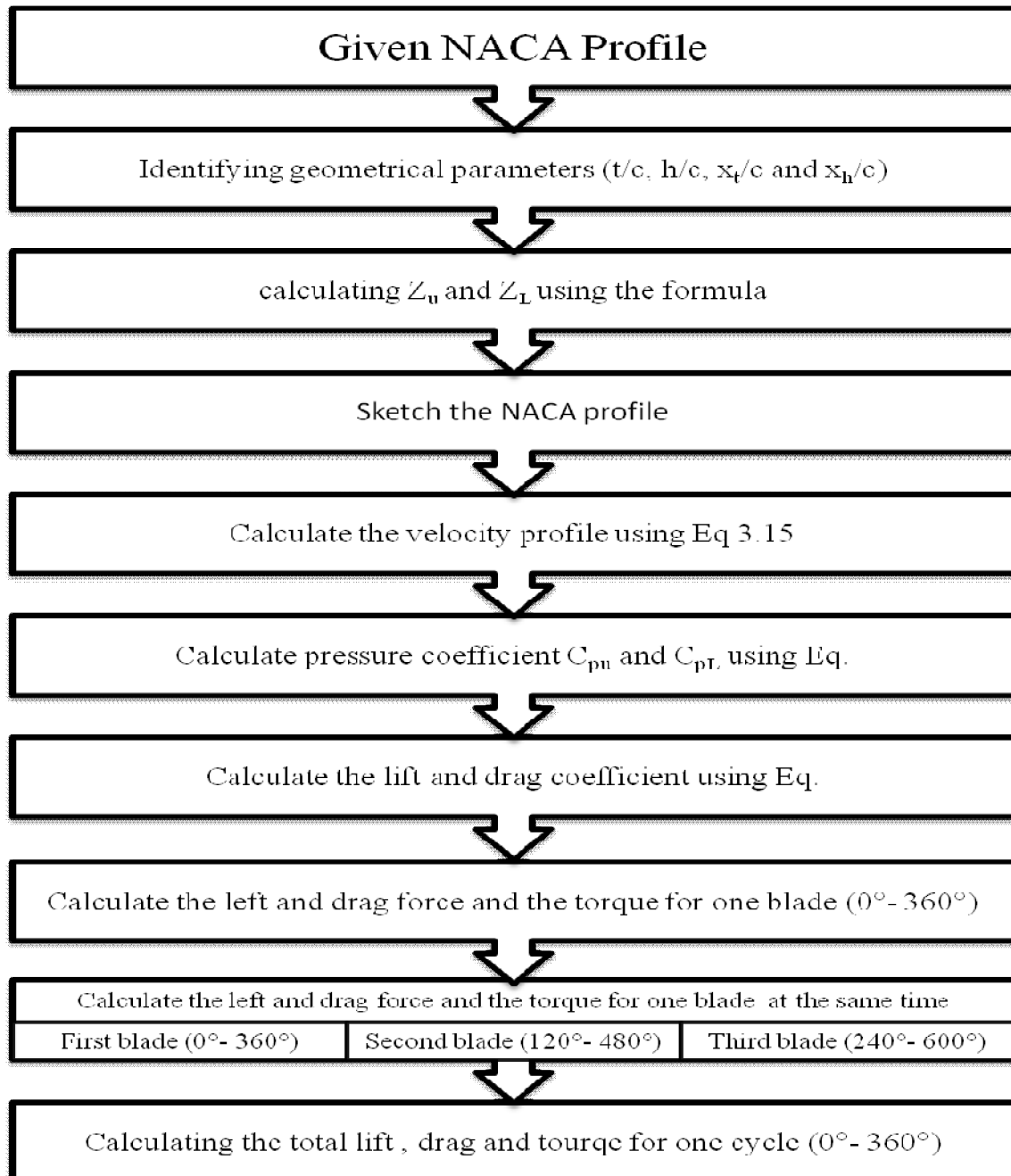


Figure 4.7 Relation between the angle of rotation (γ) and the forces of the profiles

4.3 Flowchart for the calculation of the Forces and Torques of Wind Car

A flowchart is a type of diagram that represents an algorithm or process, showing the steps as boxes of various kinds, and their order by connecting them with arrows. This diagrammatic representation can give a step-by-step solution to a given problem. Process operations are represented in these boxes, and arrows connecting them represent flow of control.



As given in NACA profile we can identify the geometric parameters of the airfoil

- t/c : relative thickness (thickness ratio)
- h/c : relative camber (camber ratio)
- x_t/c : relative thickness position
- x_h/c : relative camber position

then Eq.2.1a or 2.1b are used to calculate symmetrical 4-digit NACA airfoil and Eq.2.2 is used to calculate the mean camber line. Figure 4.8 represents the coordinates Z_u of the upper airfoil surface and Z_L of the lower airfoil surface for four different types of airfoils. The equations used to calculate Z_u and Z_L are given by formula 4.2.

$$Z_u = z^c + z^t \quad \text{and} \quad z_L = z^c - z^t \quad 4.2$$

Where,

z^c : coordinates of mean camber line

z^t : coordinates of the symmetrical 4-digit NACA airfoil

Z_u : coordinates of the upper airfoil surface

Z_L : coordinates of the lower airfoil surface

After the calculation of the upper and lower surfaces we can sketch the airfoil as shown in figure 4.18. Then using Eq. 3.16 we can calculate the velocity distribution. The pressure coefficient of the profile is given by:

$$C_p = 1 - \left(\frac{W_k}{U_\infty} \right)^2 \quad 4.3$$

After that using Eqs. 3.13 and 3.14 we can calculate the lift and drag coefficients respectively. Further more, we can calculate the lift and drag by using Eqs. 2.50 and 2.51 respectively for one blade and then for three blades at the same time; where the first, second and third blades are

between 254° and 270° . We can calculate the total lift and drag forces for all the blades at the same positions using Eqs. 4.4 and 4.5. At the end, we calculate the total torque for the blades from 0° to be 360° . More explanations are given in the flow chart of NACA airfoils.

$$F_L(\text{total}) = F_L(\text{first blade}) + F_L(\text{second blade}) + F_L(\text{third blade}) \quad 4.4$$

$$F_D(\text{total}) = F_D(\text{first blade}) + F_D(\text{second blade}) + F_D(\text{third blade}) \quad 4.5$$

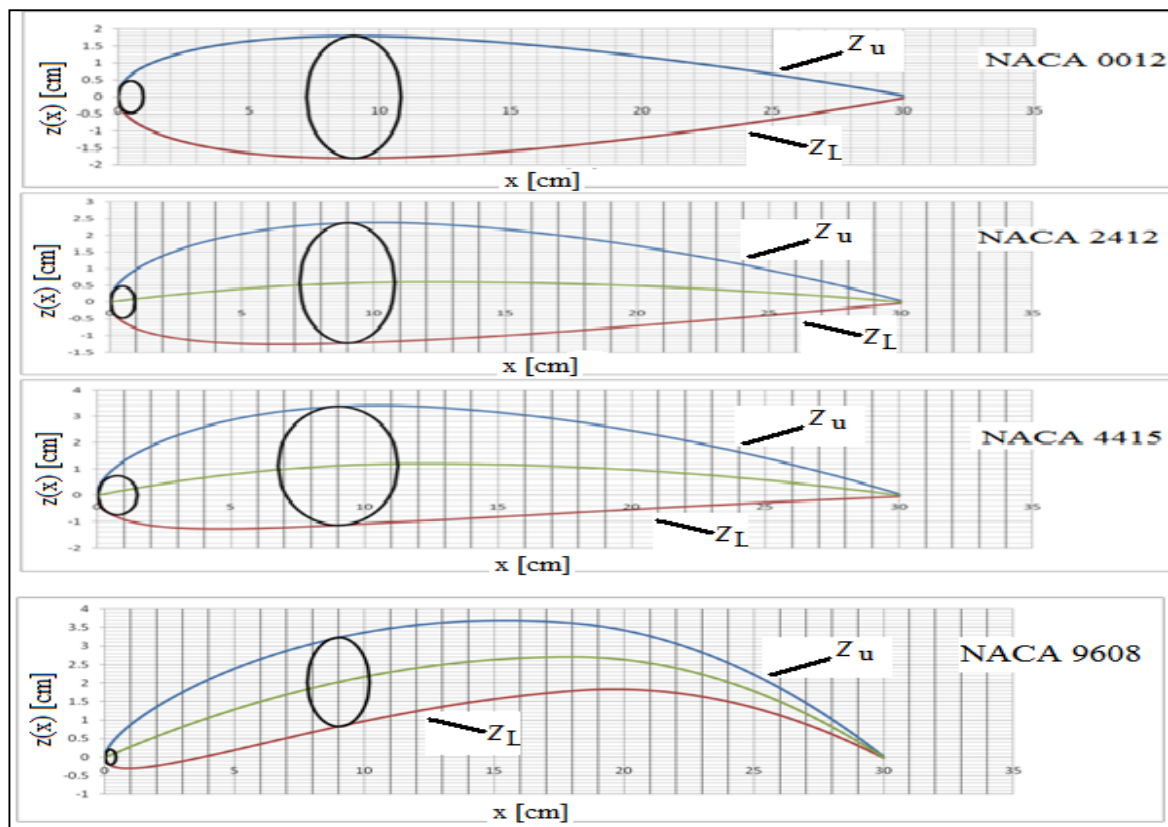


Figure 4.8 The coordinate of upper and lower surfaces for different types of airfoils

Using the flow chart of four digit NACA airfoils we can calculate the velocity distribution, pressure, lift and drag coefficient. The total forces and the torque for different NACA profiles also can be calculated using the same flowchart. The lift and drag forces acting on each one of the airfoils were successfully calculated with an airflow velocity of 4 m/s and speed of the blade

of 13.056m/s [29]. The NACA 0012 is a symmetrical airfoil with a 12% thickness to chord ratio. When the airfoil is located in a stream of air of velocity U_∞ , the flow has to pass near the leading edge and along the upper and the lower airfoil surface. At the location where the flow is splitting up, the flow velocity is reduced to zero. This point is called stagnation point. It is located close to the leading edge of the airfoil, but its position moves with the angle of attack. Table 4.3 represents the lift coefficient and the relative error in percentage (R.E) between the theoretical and calculated values for NACA 0012. Figures 4.11-4.16 show the change in lift, drag forces and the torque for NACA 0012 profiles with angle of rotation (γ).

Table 4.1 Velocity distribution data for both surfaces of the NACA 0012 airfoil at 2° angle of attack

X	w/U_∞ upper	w/U_∞ lower
0.983	0.919	0.9116
0.933	0.9697	0.9533
0.8536	1.0174	0.9907
0.75	1.0585	1.0196
0.6294	1.0988	1.0451
0.5	1.1415	1.0691
0.3706	1.1941	1.0834
0.25	1.2372	1.104
0.1464	1.2818	1.0929
0.067	1.3249	1.0351
0.017	1.3293	0.7992

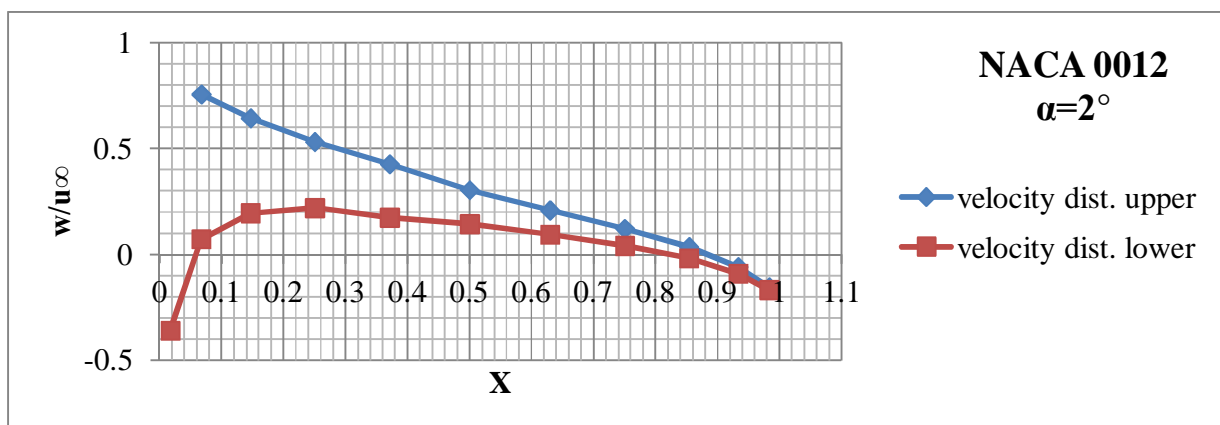


Figure 4.9 Velocity distribution plot for both surfaces of the NACA 0012 airfoil at 2° angle of attack.

Table 4.2 Pressure coefficient data for both surfaces of the NACA 0012 airfoil at 2° angle of attack

X	-Cp upper	-Cp lower
0.983	-0.1554	-0.169
0.933	-0.0596	-0.0911
0.8536	0.0352	-0.0186
0.75	0.1205	0.0395
0.6294	0.2074	0.0922
0.5	0.3031	0.1429
0.3706	0.4259	0.1737
0.25	0.5308	0.2188
0.1464	0.643	0.1944
0.067	0.7554	0.0714
0.017	0.7669	-0.3613

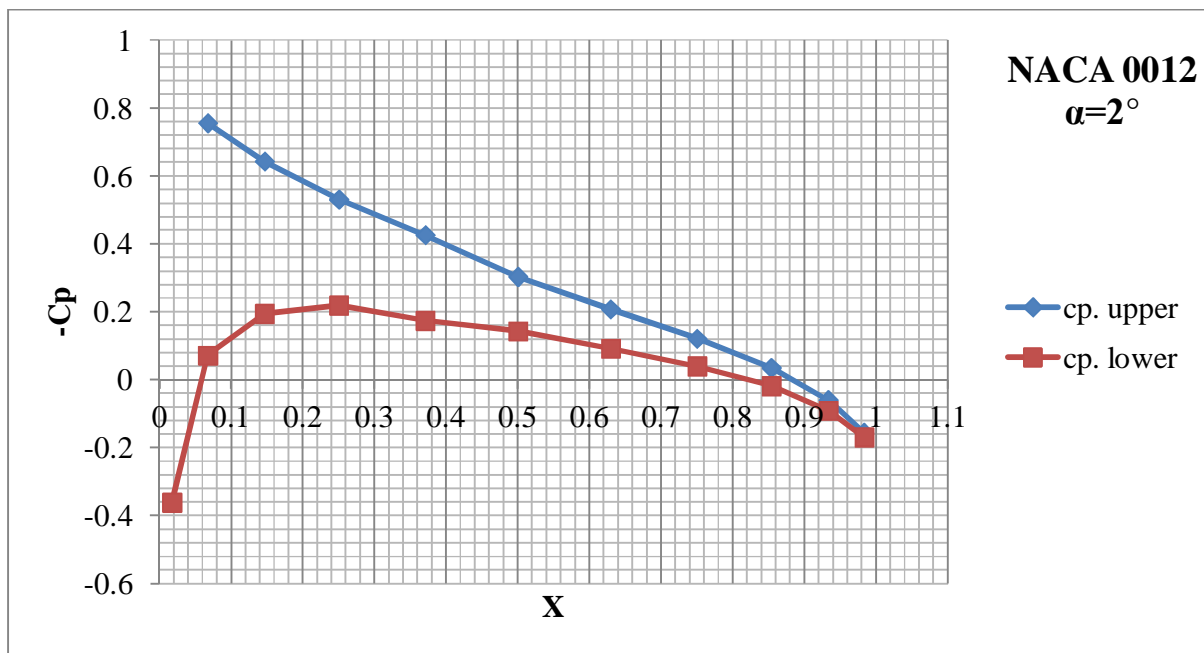


Figure 4.10 Pressure coefficient plot for both surfaces of the NACA 0012 airfoil at 2° angle of attack

Table 4.3 Lift coefficient (C_L) of NACA 0012 airfoil at varying angle of attack

Angle of attack (α) [°]	C_L (Theoretical)	C_L (Calculated)	Relative Error in Percentage $R. E = \left \frac{\text{theoretical} - \text{calculated}}{\text{theoretical}} \right \times 100$
2°	0.237	0.2302	2.869%
4°	0.473	0.4574	3.298%
6°	0.708	0.6808	3.841%
8°	0.942	0.8994	4.522%
10°	1.175	1.1125	5.319%
12°	1.404	1.3193	6.032%
14°	1.632	1.5190	6.924%

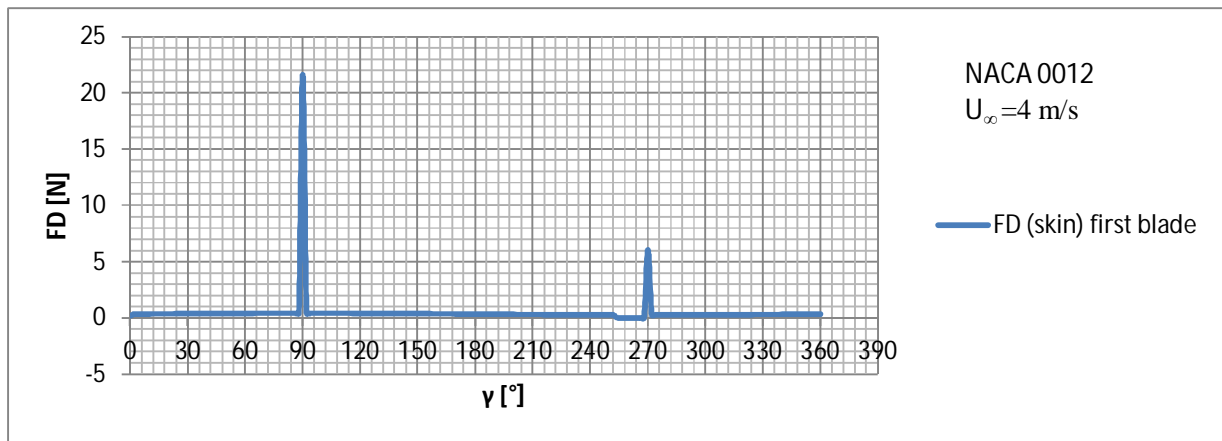


Figure 4.11 Skin friction drag force for one blade plot of the NACA 0012 airfoil.

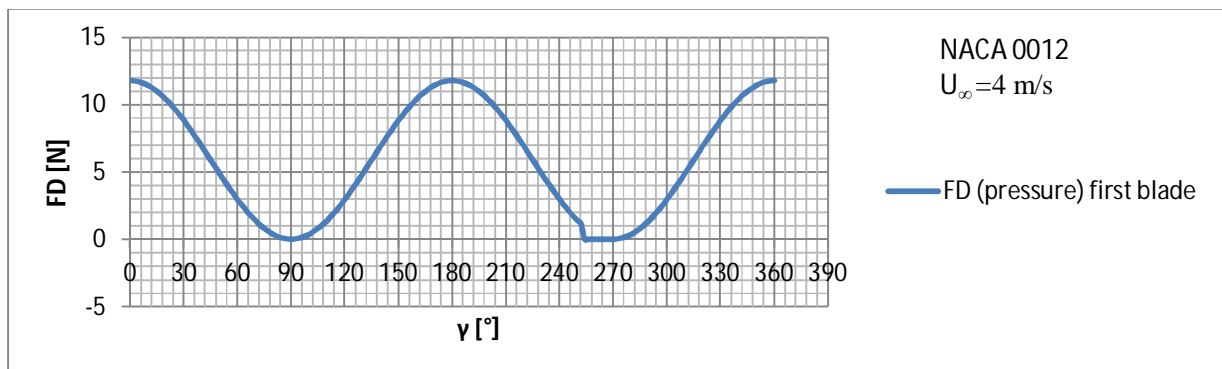


Figure 4.12 Pressure drag force for one blade plot of the NACA 0012 airfoil.

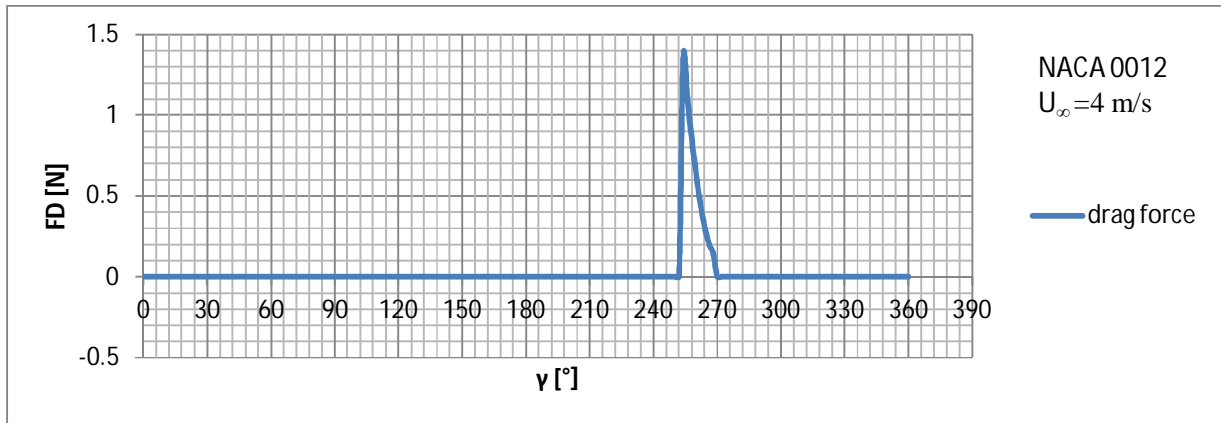


Figure 4.13 Drag force for one blade plot of the NACA 0012 airfoil.

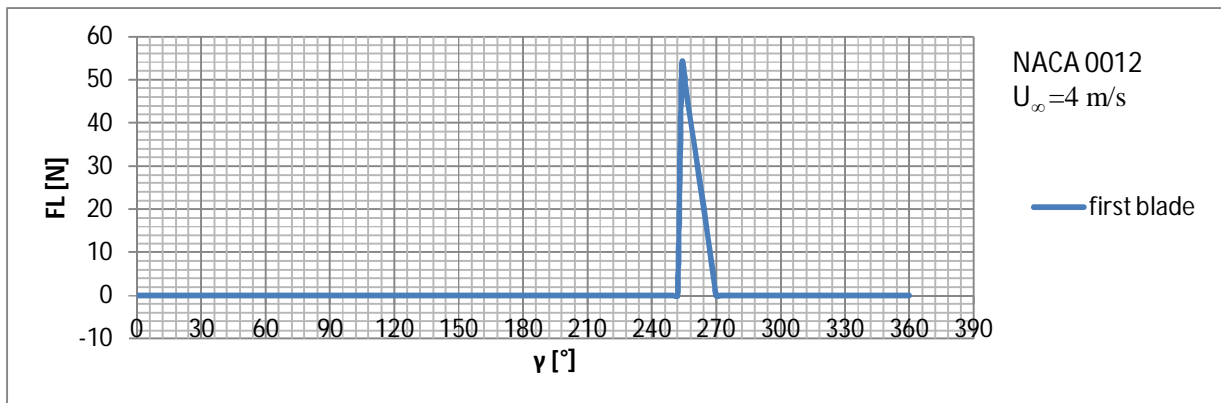


Figure 4.14 lift force for one blade plot of the NACA 0012 airfoil.

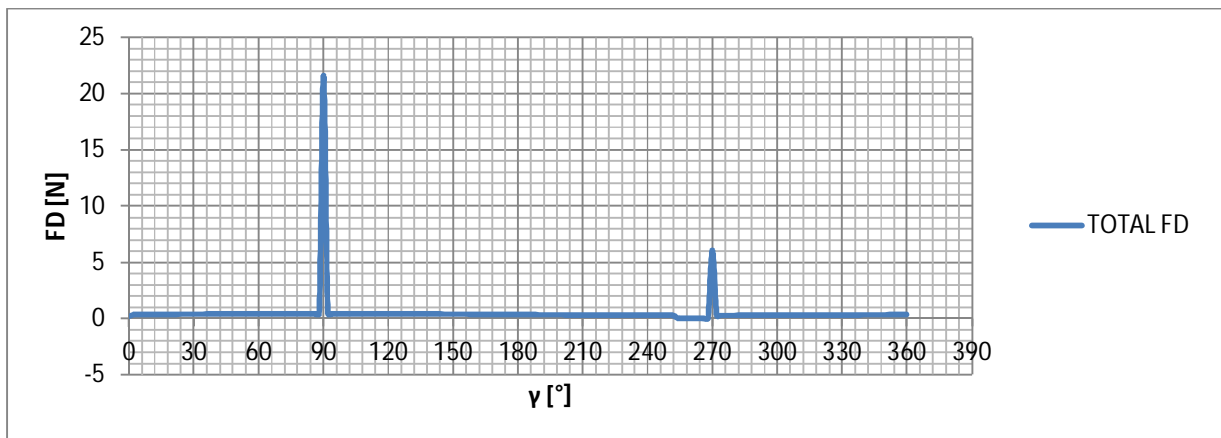


Figure 4.15 total skin friction forces for one blade plot of the NACA 0012 airfoil.

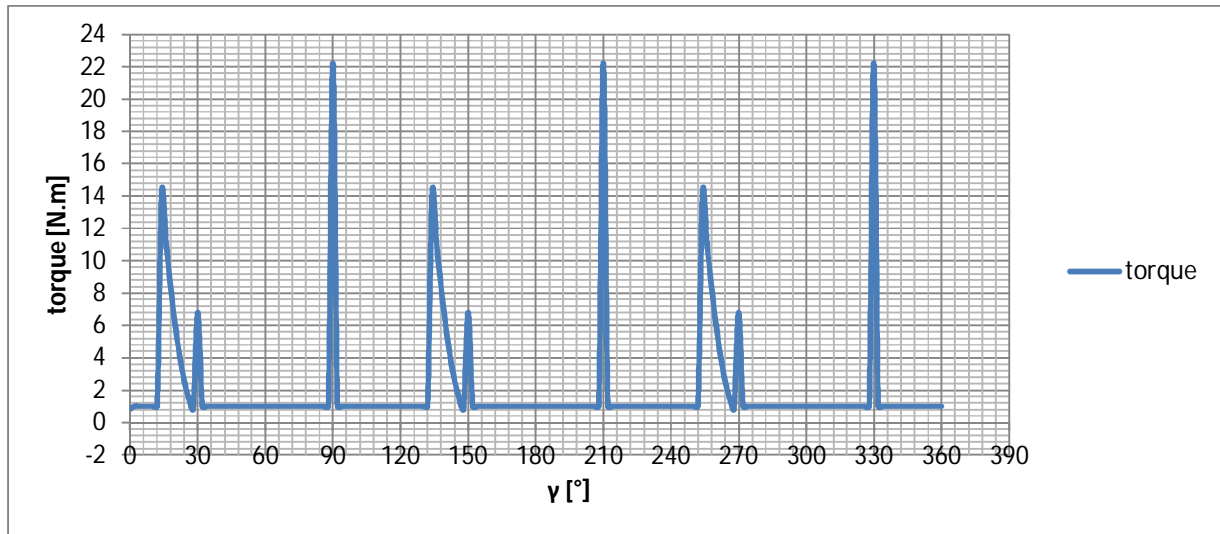


Figure 4.16 Torque plot of the NACA 0012 airfoil.

Using the same procedure (Flow chart) to calculate the velocity distribution, pressure, lift and drag coefficient, the forces and the torque for different NACA profiles. NACA 2412 airfoil has a maximum thickness of 12% with a camber of 2% located 40% back from the airfoil leading edge. NACA 4415 airfoil has a maximum thickness of 15% with a camber of 4% located 40% back from the airfoil leading edge. NACA 9608 airfoil has a maximum thickness of 8% with a camber of 9% located 60% back from the airfoil leading edge. Table 4.4 shows the lift coefficient for three types of airfoils.

Table 4.4 Lift coefficient for three types of airfoils

NACA profile	Lift coefficient
NACA 2412	0.4932
NACA 4415	0.7618
NACA 9608	1.6

Table 4.5 Velocity distribution data for both surfaces of the NACA 4415 airfoil at 2° angle of attack

X	w/U _∞ upper	w/U _∞ lower
0.983	0.9276	0.8569
0.933	1.0191	0.8801
0.8536	1.1046	0.9012
0.75	1.1771	0.917
0.6294	1.2439	0.9333
0.5	1.3089	0.9528
0.3706	1.3929	0.9537
0.25	1.4378	0.9885
0.1464	1.4523	1.0112
0.067	1.4297	0.9968
0.017	1.2876	0.7954

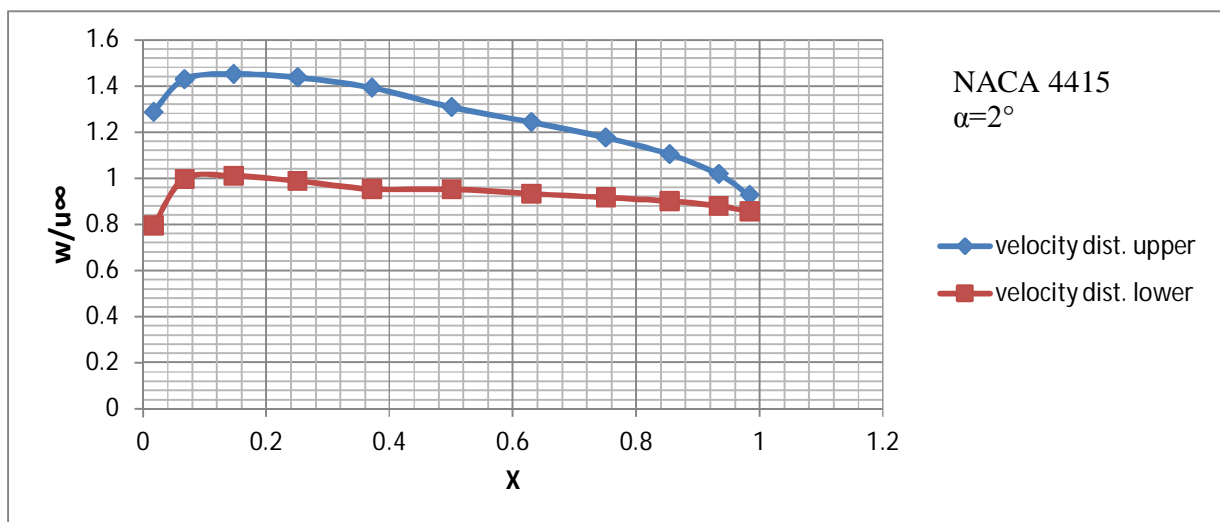


Figure 4.17 Velocity distribution plot for both surfaces of the NACA 4415 airfoil at 2° angle of attack.

Table 4.6 Pressure coefficient data for both surfaces of the NACA 4415 airfoil at 2° angle of attack

X	-Cp upper	-Cp lower
0.983	-0.1396	-0.2657
0.933	0.0386	-0.2255
0.8536	0.2201	-0.1878
0.75	0.3855	-0.1592
0.6294	0.5474	-0.129
0.5	0.7132	-0.0921
0.3706	0.94	-0.0905
0.25	1.0672	-0.0229
0.1464	1.1091	0.0225
0.067	1.044	-0.0064
0.017	0.6579	-0.3673

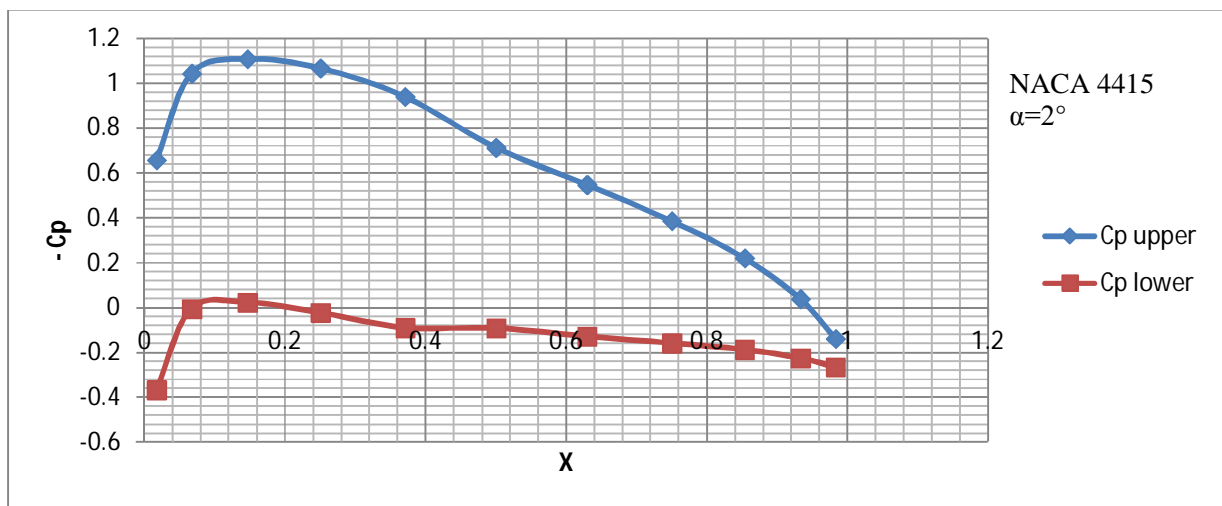


Figure 4.18 Pressure distribution plot for both surfaces of the NACA 4415 airfoil at 2° angle of attack.

Table 4.7 Velocity distribution data for both surfaces of the NACA 2412 airfoil at 2° angle of attack

X	w/U_∞ upper	w/U_∞ lower
0.983	0.935	0.8956
0.933	1.0007	0.9224
0.8536	1.0619	0.9462
0.75	1.1141	0.964
0.6294	1.1632	0.9807
0.5	1.2124	0.9982
0.3706	1.275	1.0025
0.25	1.3155	1.0257
0.1464	1.3439	1.0308
0.067	1.3601	0.9999
0.017	1.3239	0.8046

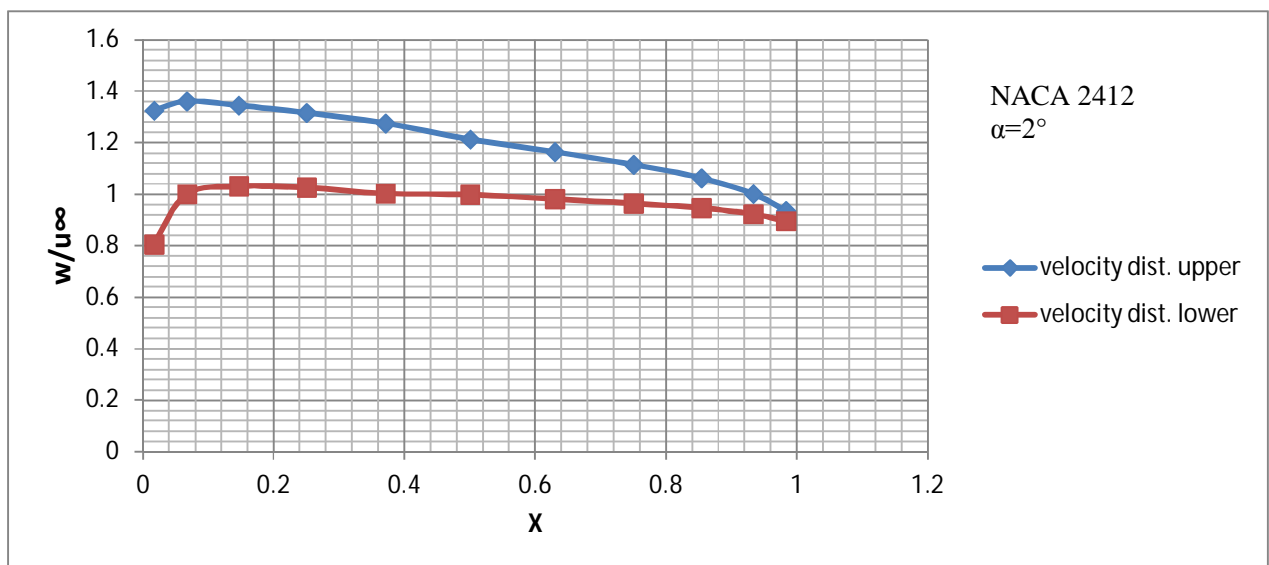


Figure 4.19 Velocity distribution plot for both surfaces of the NACA 2412 airfoil at 2° angle of attack

Table 4.8 Pressure coefficient data for both surfaces of the NACA 2412 airfoil at 2° angle of attack

X	-Cp upper	-Cp lower
0.983	-0.1257	-0.1979
0.933	0.0014	-0.1492
0.8536	0.1276	-0.1047
0.75	0.2412	-0.0707
0.6294	0.353	-0.0382
0.5	0.4698	-0.0035
0.3706	0.6256	0.0049
0.25	0.7305	0.0521
0.1464	0.806	0.0626
0.067	0.8498	-0.0001
0.017	0.7526	-0.3526

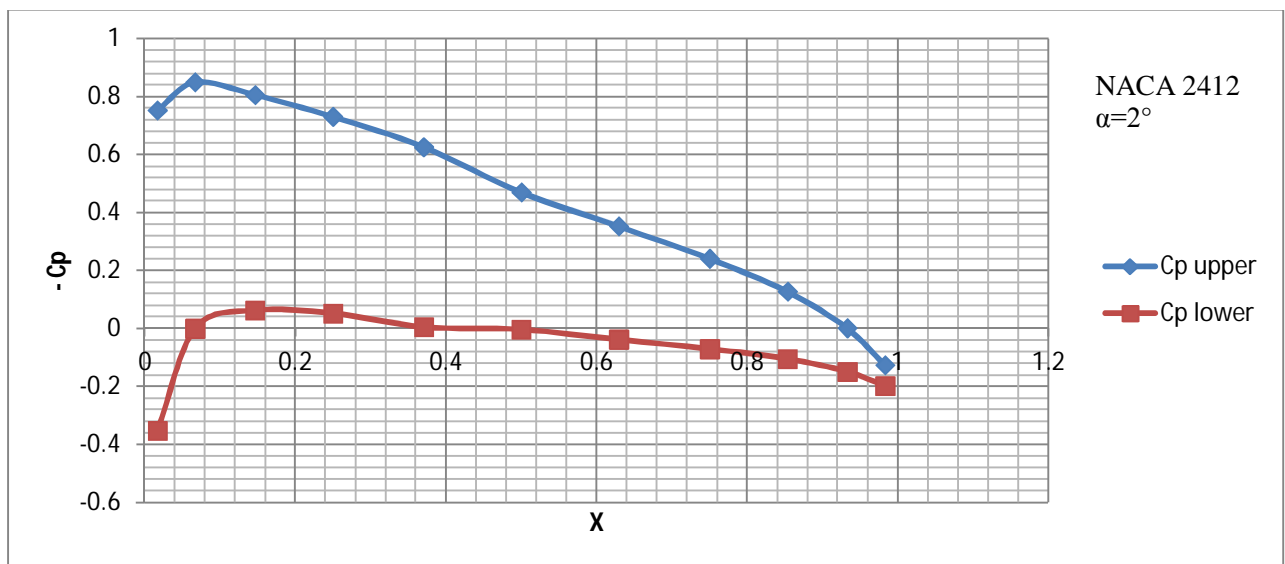


Figure 4.20 Pressure distribution plot for both surfaces of the NACA 2412 airfoil at 2° angle of attack

Table 4.9 Velocity distribution data for both surfaces of the NACA 9608 airfoil at 2° angle of attack

X	w/U_∞ upper	w/U_∞ lower
0.983	1.0759	0.8137
0.933	1.2275	0.7247
0.8536	1.355	0.6536
0.75	1.445	0.6096
0.6294	1.4811	0.6167
0.5	1.466	0.6755
0.3706	1.4773	0.7079
0.25	1.4764	0.7512
0.1464	1.4757	0.7774
0.067	1.4876	0.7687
0.017	1.5627	0.5915

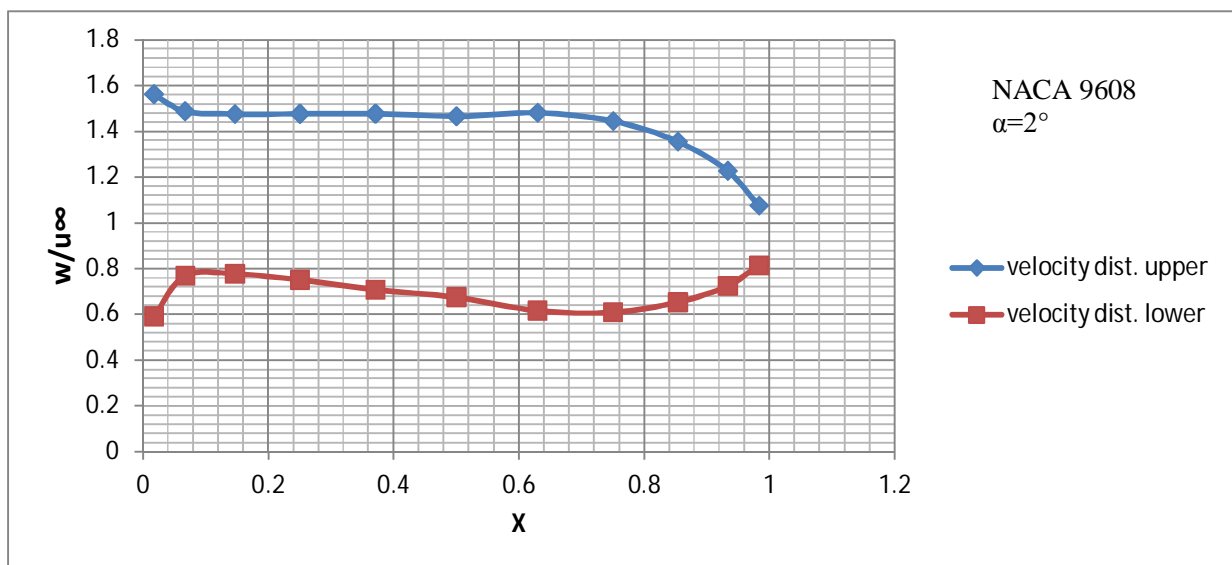


Figure 4.21 Velocity distribution plot for both surfaces of the NACA 9608 airfoil at 2° angle of attack

Table 4.11 Pressure coefficient data for both surfaces of the NACA 9608 airfoil at 2° angle of attack

X	-Cp upper	-Cp lower
0.983	0.1575	-0.3379
0.933	0.5067	-0.4748
0.8536	0.836	-0.5728
0.75	1.0879	-0.6283
0.6294	1.1937	-0.6197
0.5	1.1491	-0.5438
0.3706	1.1823	-0.4989
0.25	1.1798	-0.4357
0.1464	1.1778	-0.3957
0.067	1.2131	-0.4091
0.017	1.442	-0.6501

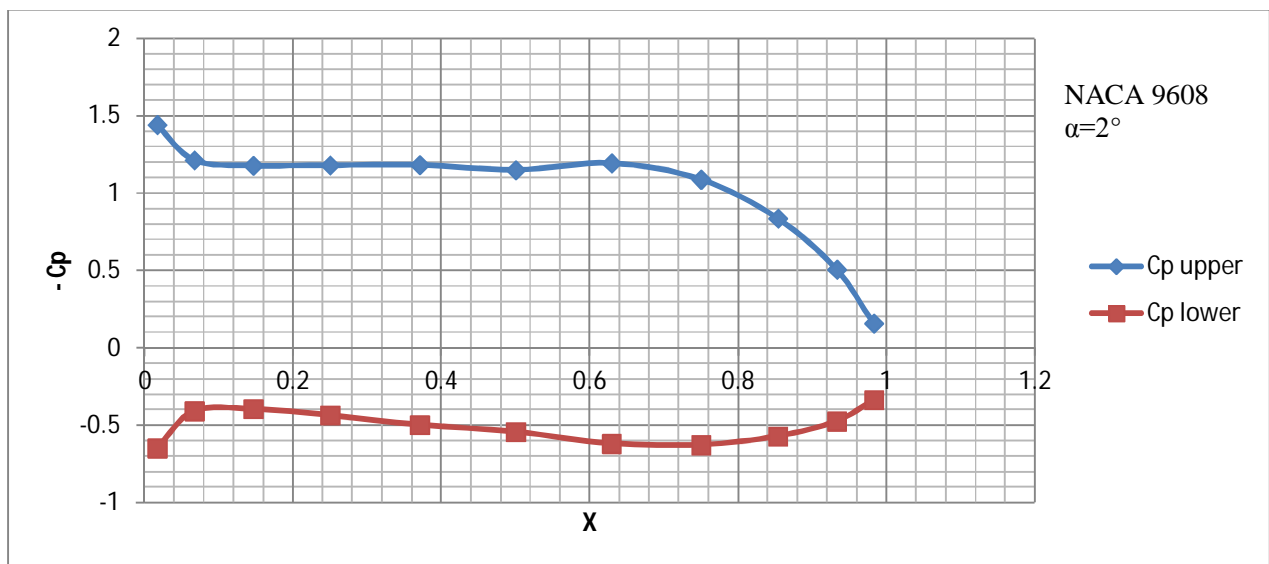


Figure 4.22 Pressure distribution plot for both surfaces of the NACA 9608 airfoil at 2° angle of attack

The lift coefficient of an airfoil depends not only on the angle of attack, but also on the shape of the airfoil, the plan area of the airfoil (or wing area), the square of the velocity, and the density of the air.

Table 4.11 shows a typical comparison between both theoretical analysis method and calculated results at low-speed and the relative error in percentage.

Table 4.11 Lift coefficient (C_L) of NACA airfoils at 2° angle of attack

NACA Profiles	C_L (Theoretical)	C_L (Calculated value)	Relative Error in Percentage
NACA 0012	0.237	0.2302	2.86%
NACA 2412	0.479	0.4932	2.96%
NACA 4415	0.729	0.7618	4.49%
NACA 9608	1.31	1.6	22.13%

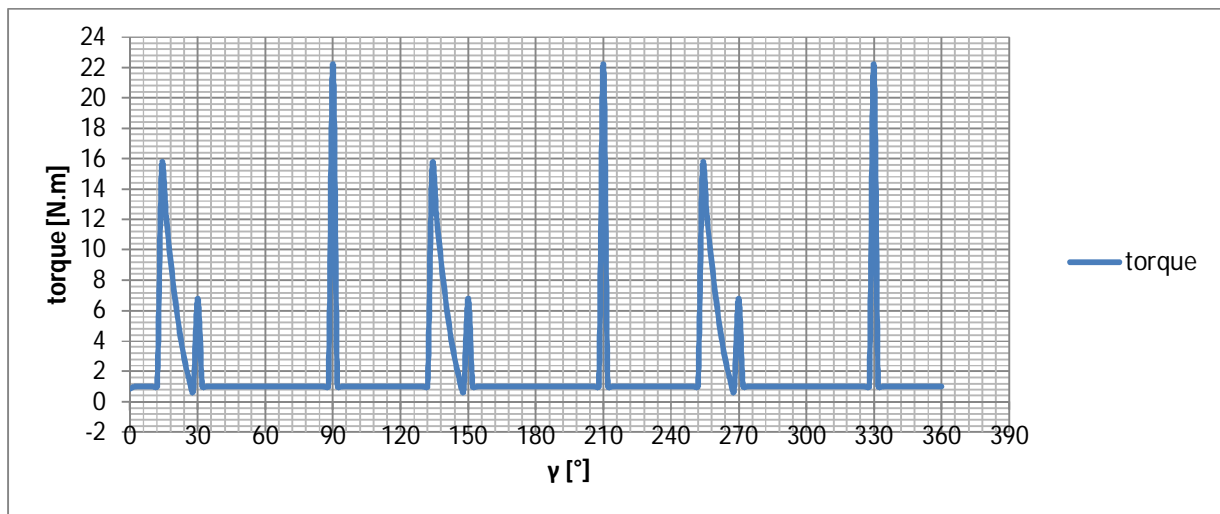


Figure 4.23 Torque plot of the NACA 2412 airfoil.

CHAPTER 5

CONCLUSIONS AND FUTURE WORK

The airfoils chosen for this work were the NACA 0012, NACA 2412, NACA 4415, and NACA 9608. In this work, airfoils are characterized under the low-speed operation conditions. The data obtained from this work was then analyzed in order to obtain values for the coefficient C_L , C_D , to calculate the lift and drag forces and to calculate the torque.

In this work, the lift coefficient of NACA airfoils was analyzed using numerical integration of the pressure distribution. The relationship between the lift coefficient and the angle of attack is complex and can only be determined by experimentation or complicated analysis. The lift coefficient calculated using this method agreed very closely with the theoretical values created by Aerofoil.

In our work, we calculated the velocity distribution, pressure, lift coefficient, forces and the torque for NACA 2412. And we compared the results of with NACA 0012 airfoil, we found that NACA 2412 has a maximum torque but with maximum error in lift coefficient compared to NACA 0012.

Through the calculation for lift coefficient for different NACA airfoils, we found the maximum lift coefficient at 2° angle of attack for NACA9608. Also we found the maximum error for NACA 9608 because it has maximum camber line.

We found some error between the theoretical and calculated values. This error occurs during the calculation because we used eleventh node (depend on the theory). If more nodes will be used, the error can be reduced. Also to reduce the error in our work; we can use thin airfoil for example NACA 0012.

In order to prove the validity of our results, experimentation is indispensable. The work of this thesis offers more opportunities to expand this work and study more complicated profiles, or even in courage the researches for new profiles which ameliorate the flow condition. The use wind tunnel can give better results for the forces. Wind tunnel is used to simulate airflow over a model of airplane or a wing section so it can be studied. The wind tunnel can produce air flow at the desired speed and condition.

REFERENCES

- [1] E. L. Hought, and P.W.Carpenter, (2003) Aerodynamics for Engineering Student. Fifth edition, Great Britain: Butterworth-Heinemann
- [2] Dr. Mustafa Cavcar, (2003) Basic Aerodynamics-subject12-Revised on [16 /4/2003], home.anadolu.edu.tr/~mcavcar/hyo301/12_AirfoilTerminology.pdf , [accessed 04/05/2011]
- [3] Civil Air Patrol, Educational Materials, (December 23, 2008) Aeronautics- Principles of flight (Airfoil)-Level 2, <http://www.allstar.fiu.edu/aero/flight31.htm> [accessed 11/06/2011].
- [4] everything, <http://everything2.com/title/mean+camber+line>, [accessed 11/06/2011].
- [5] Marzocca, Pier, "The NACA airfoil series" ,Clarkson University. Retrieved 07-03-2009.
- [6] H. Schlichting, and E.Truckenbrodt, (1979) Aerodynamic of the Airplane, United state of America.
- [7] Dr. Ganesh Rajagopalan, (2005) INCOMPRESSIBLE FLOW OVER AIRFOILS, www.public.iastate.edu/~rajagopa/2006F/pdf-files/chap7.pdf, [accessed 20/09/2011].
- [8] Wikipedia,. http://en.wikipedia.org/wiki/Kutta_condition [accessed 11/06/2011].
- [9] Wikipedia, Aeroforces.sv. <http://en.wikipedia.org/wiki/File:Aeroforces.svg> [accessed 11/06/2011].
- [10] Alex Sullivan,(May 6, 2010) Aerodynamic forces acting on an airfoil, Physics Department; The College of Wooster; Wooster; Ohio; 44691; USA
- [11] Civil Air Patrol, Educational Materials, (2 October 2011) Wikipedia, http://en.wikipedia.org/wiki/Drag_coefficient [accessed 11/06/2011].
- [12] R. W. Fox and A. T. Mcdonald and P.J.Pritchard. (September 29, 2002) Introduction to Fluid Mechanics. Sixth Edition. United State.
- [13] W. P. Graebel, (2001) Engineering fluid mechanics, Great Britain
- [14] Wikipedia, Wikipedia, the free encyclopedia. http://en.wikipedia.org/wiki/Lift_Coefficient [accessed 11/06/2011].
- [15] Carriere, P., E. Eichelbrenner, and P. Poisson-Quinton: Contribution theorique et experimentale a l'etude du controle de la couche limitee par soufflage, Adv. Aer. Set, 2:620-

- 661,1959.
- [16] Goradia, S. H. and G. T. Colwell: Analysis of High-Lift Wing Systems, *Aer. Quart.*, 26:88-108, 1975. Foster, D. N.: *J. Aircr.*, 9:205-210, 1972.
 - [17] Jacob, K. and F. W. Riegels: Berechnung der Druckverteilung endlich dicker Profile ohne und mit Klappen und Vorflügeln, *Z. Flugw.*, 11:357-367, 1963.
 - [18] Nonweiler, T.: Maximum Lift Data for Symmetrical Wings-A Resume of Maximum Lift Data for Symmetrical Wings, Including Various High-Lift Aids, *Aircr. Eng.*, 27:2-8, 1955; 28:216-227, 1956.
 - [19] Arnold, K. O.: Aerodynamische Untersuchungen an Flügel mit Bremsklappen, *Z. Flugw.*, 14:276-281, 1966. Fuchs, D.: *Lufo.*, 15:19-27, 1938. Jacobs, H. and A. Wanner: *Jb. Lufo.*, 1:313-318, 1938. Rellei, E.: *ZWB Lufo. FB 1689/1*, 1942; *1689/2*, 1943. Voepel, H.: *Jb. Lufo.*, 1:82-95, 1941. Wanner, A.: *Jb. Lufo.*, 1:308-312, 1940
 - [20] Wenzinger, C. I.: Wind-Tunnel Investigation of Ordinary and Split Flaps on Airfoils of Different Profile, *NACA Rept. 554*, 1936
 - [21] Seiferth, R.: Kraftmessungen und Druckverteilungsmessungen an zwei Flügeln mit Klappe und Diisenspalt, *Jb. Lufo.*, 1:36-51, 1941; 1:84-87, 1939. Kiel, G.: *Lufo.*, 14:71-84, 1937. Ruden, P.: *Jb. Lufo.*, 1:75-86, 1937.
 - [22] Wenzinger, C. I.: Wind-Tunnel Investigation of Ordinary and Split Flaps on Airfoils of Different Profile, *NACA Rept. 554*, 1936.
 - [23] Wenzinger, C. J. and F. M. Rogallo: Wind-Tunnel Investigation of Spoiler, Deflector, and Slot Lateral-Control Devices on Wings with Full-Span Split and Slotted Flaps, *Rept. 706*, 1941.
 - [24] E. L. Houghto, and P.W.Carpenter, (2003) *Aerodynamics for Engineering Student*. Fifth edition, Great Britain: Butterworth-Heinemann
 - [25] L J Clancy, 1975, *Pitman Aeronautical Engineering Series*, John Wiley & Sons, Inc., pp. 54-115
 - [26] David Heffley, (2007) *Aerodynamic characteristics of NACA 4412 airfoil*, Mechanical Engineering department, Baylor University
 - [27] Young, A. D.: *The Aerodynamic Characteristics of Flaps*, *ARC RM 2622*, 1947/1953
 - [28] Aerospace, <http://www.aerospaceweb.org/question/airfoils/q0259c.shtml>, [accessed 17/09/2011].

[29] Kazim Temiz, (2010), Design and production of wind car, Bsc, Near East University

APPENDICES

MATLAB (matrix laboratory) is a numerical computing environment. MATLAB allows matrix manipulations, plotting of functions and data, implementation of algorithms. We use it to draw the velocity, pressure distribution, lift coefficient and force as shown below.

```
clc;
clear all;
L=30;
% free stream velocity
U_infin=10;
density=1.23;
R=1;
aera=(L*R)/100;
% alpha: angle of attack
alpha=(2*pi)/180;
% d_L: maximum thickness
d_L=0.12;
% Xf_L: location of maximum camber
Xf_L=0.4;
% f_L: maximum camber
f_L=0.02;
N=12;
angle_rad=( [ 15 30 45 60 75 90 105 120 135 150 165 ]*pi)/180;
Xm=0.5*(1+cos(angle_rad));
a0=1.4845;
a1=-0.6300;
a2=-1.7580;
a3=1.4215;
a4=-0.5075;
gumaa=30;

% Zmt : Equation for a symmetrical
Zmt=(d_L)*((a0.*(Xm).^0.5)+(a1.*Xm)+(a2.*Xm.^2)+(a3.*Xm.^3)+(a4.*Xm.^4));

% Zms: mean camber line
% Zms for symmetrical
% Zms=0;
% Zms for unsymmetrical
for i=1:11
    if Xm(i)<=Xf_L,
        Zms(i)=f_L/Xf_L^2*(2*Xf_L*Xm(i)-Xm(i)^2);
    else
        Zms(i)=(f_L/(1-Xf_L)^2)*(1-2*Xf_L+2*Xf_L*Xm(i)-Xm(i)^2);
    end;
end;
% Z_up :upper surface
% Z_lower: lower surface
Z_up=(Zmt+Zms);
Z_lower=(-Zmt+Zms);
figure (1)
plot(Xm,Zms); xlabel('Xm'); ylabel('Zms');
```

```

cn=[ 0.0168 0.0625 0.125 0.1875 0.2333 0.25 0.2333 0.1875 0.125 0.0625 0.0168
];
an=[ 0.1294 0.25 0.3536 0.433 0.483 0.5 0.483 0.433 0.3536 0.25 0.1294 ];
bn=[ 0.017 0.067 0.1464 0.25 0.3706 0.5 0.6294 0.75 0.8536 0.933 0.983 ];
der_xm=-0.5.*sin(angle_rad);

```

```

Zmt_angle=(d_L)*(a0*0.5*Xm.^-0.5.*der_xm + a1.*der_xm + a2*2.*Xm.*der_xm
+ a3*3.*Xm.^2.*der_xm + a4*4.*Xm.^3.*der_xm);

```

```

A=[ 3 -1.0806 0 -0.086 0 -0.0231 0 -0.0087 0 -0.0032 0 ; -1.0806 3 -1.1666 0
-0.1092 0 -0.0318 0 -0.0119 0 -0.0032 ;...
0 -1.1666 3 -1.1897 0 -0.1179 0 -0.035 0 -0.0119 0 ; -0.086 0 -1.1897 3 -
1.1984 0 -0.1211 0 -0.035 0 -0.0087 ;...
0 -0.1092 0 -1.1984 3 -1.2016 0 -0.1211 0 -0.0318 0 ; -0.0231 0 -0.1179 0 -
1.2016 3 -1.2016 0 -0.1179 0 -0.0231 ;...
0 -0.0318 0 -0.1211 0 -1.2016 3 -1.1984 0 -0.1092 0 ; -0.0087 0 -0.035 0 -
0.1211 0 -1.1984 3 -1.1807 0 -0.086 ;...
0 -0.0119 0 -0.035 0 -0.1179 0 -1.1897 3 -1.1666 0 ; -0.0032 0 -0.0119 0 -
0.0318 0 -0.1092 0 -1.1666 3 -1.0806 ;...
0 -0.0032 0 -0.0087 0 -0.0231 0 -0.086 0 -1.0806 3 ];

```

```

C=[ 5.4454 -1.3651 0.2845 -0.1985 0.1124 -0.0893 0.0662 -0.0575 0.0488 -
0.0456 0.0424 ;...
1.0806 3 -0.9945 0 -0.0629 0 -0.0144 0 -0.0055 0 -0.0032 ;...
2.4457 -1.279 3.2845 -1.2559 0.1124 -0.1667 0.0662 -0.0774 0.0488 -0.0543
0.0424 ;...
2.2475 0 -0.9714 3 -1.1348 0 -0.0973 0 -0.0286 0 -0.0151 ;...
2.4457 -0.1754 0.2845 -1.2472 3.1124 -1.244 0.0662 -0.1635 0.0488 -0.0806
0.0424 ;...
2.3563 0 0.1179 0 -1.1316 3 -1.1778 0 -0.1179 0 -0.0469 ;...
2.4457 -0.0806 0.2845 -0.1635 0.1124 -1.244 3.0662 -1.2472 0.0488 -0.1754
0.0424 ;...
2.3882 0 0.2071 0 -0.051 0 -1.181 3 -1.2071 0 -0.1561 ;...
2.4457 -0.0543 0.2845 -0.0774 0.1124 -0.1667 0.0662 -1.2559 3.0488 -1.2790
0.0424 ;...
2.4001 0 0.2302 0 0.0318 0 -0.1092 0 -1.2302 3 -1.3227 ;...
2.4457 -0.0456 0.2845 -0.0575 0.1124 -0.0893 0.0662 -0.1985 0.0488 -1.3651
3.0424 ];

```

```

H=[ 0.7113 -0.3544 0.1003 -0.0910 0.0538 -0.0469 0.0301 -0.0262 0.0155 -
0.0120 0 ;...
0.1422 0.8039 -0.4119 0 -0.0483 0 -0.0188 0 -0.0132 0 -0.0244 ;...
0.3155 -0.3296 1.3403 -0.6969 0.0488 -0.1178 0.0227 -0.0495 0 -0.0204 -
0.0488 ;...
0.2958 0 -0.4024 1.7321 -0.8708 0 -0.1267 0 -0.069 0 -0.1148 ;...
0.3133 -0.0293 0.0904 -0.6820 2.3375 -1.1778 0 -0.1685 -0.042 -0.0539 -
0.1808 ;...
0.3102 0 0.0488 0 -0.8683 3 -1.535 0 -0.2845 0 -0.3565 ;...
0.3072 0.0085 0.0713 -0.0295 0 -1.1316 3.8495 -1.19656 -0.1535 -0.2349 -
0.5319 ;...
0.3144 0 0.0858 0 -0.0392 0 -1.5392 5.1962 -2.9142 0 -1.1865 ;...

```

```

0.2845 0.0617 0 0.1196 -0.1320 0.1178 -0.2845 -1.6826 6.6737 -3.7117 -1.839
;...
0.316 0 0.0954 0 0.0244 0 -0.1423 0 -2.97 11.1962 -10.0469 ;...
0 0.6431 -0.8952 1.3788 -1.7903 2.3563 -3.1009 3.8922 -5.7864 4.0326 4.5328
];
m=1:11;
n=1:11;
sumA_zt=A(:,m)* Zmt';

sumC_zs=C(:,m)* Zms';

sumH_zt=H(:,m)* Zmt';

for n=1:11

    xn_star(n) =(cn(n)+Zmt_angle(n).^2).^0.5;
    velocity_des_upper(n)=(1/xn_star(n))* (an(n)+ 2* (sumA_zt(n)) +
2*(sumC_zs(n)) + alpha*(bn(n) + 2* (sumH_zt(n)))) );
    velocity_des_lower(n)=(1/xn_star(n))* (an(n)+ 2* sumA_zt(n) -
2*sumC_zs(n) - alpha*(bn(n) + 2* sumH_zt(n)) );
end;

    cp_upper=1-velocity_des_upper.^2;
    cp_upper=-cp_upper;
    cp_lower=1-velocity_des_lower.^2;
    cp_lower=-cp_lower;

Am=[0.644 0 0.2357 0 0.1726 0 0.1726 0 0.2357 0 0.6439];
Bm=[-4.8919 0 -0.5690 0 -0.2249 0 -0.1324 0 -0.0976 0 -0.0848];

% zero lift angle
sumBm_zs=Bm(:,m)*Zms';

alpha_zero=2*sumBm_zs;
sumAm_zt=Am(:,m)*Zmt';
% from table
dca_d_alpha=2*pi*(1+2*sumAm_zt);
dd=poly2sym(dca_d_alpha);
dddd=int(dd);
ddd=sym2poly(dddd);
Ca=polyval(ddd,alpha)-polyval(ddd,alpha_zero);
Ca;

F_a=0.5*U_infin^2*density*aera*Ca;
% by formula
% CP_UP_y: pressure coefficient upper in y or z direction
% CP_LO_y: pressure coefficient lower in y or z direction
% CP_UP_x: pressure coefficient upper in x direction
% CP_LO_x: pressure coefficient lower in x direction
CP_UP_y=0; CP_LO_y=0; CP_UP_x=0; CP_LO_x=0;
for i=1:10

```

```

CP_UP_y=CP_UP_y+(((cp_upper(i)+cp_upper(i+1))/2)*abs(Xm(i)-Xm(i+1)));
CP_LO_y=CP_LO_y+(((cp_lower(i)+cp_lower(i+1))/2)*abs(Xm(i)-Xm(i+1)));

CP_UP_x=CP_UP_x+(((cp_upper(i)+cp_upper(i+1))/2)*abs(Z_up(i)-Z_up(i+1)));
CP_LO_x=CP_LO_x+(((cp_lower(i)+cp_lower(i+1))/2)*abs(Z_lower(i)-
Z_lower(i+1)));

end;
% C_L_Y: lift coefficient in y or z direction
% C_L_X: lift coefficient in x direction
C_L_Y=CP_UP_y-CP_LO_y;
C_L_X=CP_UP_x-CP_LO_x;
% CL: lift coefficient
CL=C_L_Y*cos(alpha)-C_L_X*sin(alpha)
% F_L: lift force
F_L=0.5*U_infin^2*density*aera*CL

figure(2);
plot(Xm(:,1:11),velocity_des_upper,':');
hold all;
plot(Xm(:,1:11),velocity_des_lower,'ro'); hold all;
legend('velocity.des.upper','velocity.des.lower')
xlabel('Xm')
ylabel('velocity des.')
figure(3);
plot(Xm(:,1:11),cp_upper); hold all;
plot(Xm(:,1:11),cp_lower); hold all;
legend('cp.upper','cp.lower')
xlabel('Xm')
ylabel('-Cp')

d_inter=3;

x=Xm(:,1:11);
up=polyfit(x,velocity_des_upper,d_inter);
low=polyfit(x,velocity_des_lower,d_inter);
upval=polyval(up,x);
lowval=polyval(low,x);

error_v_up=velocity_des_upper-upval;
error_v_low=velocity_des_lower-lowval;

figure(4);
plot(x,upval,x,velocity_des_upper,'ro',x,error_v_up,':',x,lowval,x,velocity_d
es_lower,'mo',x,error_v_low,':');

legend('velocity.des.upper.int','velocity.des.upper','error_v_upper','velocit
y.des.lower.int','velocity.des.lower','error_v_low')
xlabel('Xm')
ylabel('velocity des.')
axis([0 1 -0.2 2.2]);

cp_up=polyfit(x,cp_upper,d_inter);
cp_low=polyfit(x,cp_lower,d_inter);

```

```
cp_upval=polyval(cp_up,x);
cp_lowval=polyval(cp_low,x);

error_cp_up=cp_upper-cp_upval;
error_cp_low=cp_lower-cp_lowval;

figure(5);
plot(x,cp_upval,x,cp_upper,'ro',x,error_cp_up,':',x,cp_lowval,x,cp_lower,'mo',
,x,error_cp_low,':');
legend('cp.upper.int','cp.upper','error_cp_up','cp.lower.int','cp.lower','err
or_cp_low')
xlabel('Xm')
ylabel('-Cp')
```